FFI RAPPORT

FIELD TEST WITH A FIBRE OPTIC SENSOR SYSTEM ON A MINE COUNTER-MEASURE VESSEL

PRAN Karianne, HAVSGÅRD Geir Bjarte, WANG Gunnar, JOHNSON Gregg, DANVER Bruce, VOHRA Sandeep

FFI/RAPPORT-99/05425

FFIE/711/116

Approved
Kjeller 1 November 1999

Stian Løvold
Director of Research

FIELD TEST WITH A FIBRE OPTIC SENSOR SYSTEM ON A MINE COUNTER-MEASURE VESSEL

PRAN Karianne, HAVSGÅRD Geir Bjarte,
WANG Gunnar, JOHNSON Gregg, DANVER Bruce,
VOHRA Sandeep

FFI/RAPPORT-99/05425

FORSVARETS FORSKNINGSINSTITUTT
Norwegian Defence Research Establishment
P O Box 25, N-2007 Kjeller, Norway

FORSVARETS FORSKNINGSINSTITUTT (FFI)
Norwegian Defence Research Establishment

P O BOX 25
2007 KJELLER, NORWAY

UNCLASSIFIED

SECURITY CLASSIFICATION OF THIS PAGE (when data entered)

REPORT DOCUMENTATION PAGE

1) PUBL/REPORT NUMBER	2) SECURITY CLASSIFICATION	3) NUMBER OF PAGES
FFI/RAPPORT-99/05425	UNCLASSIFIED	55
1a) PROJECT REFERENCE	**2a) DECLASSIFICATION/DOWNGRADING SCHEDULE**	
FFIE/711/116	-	

4) TITLE

FIELD TEST WITH A FIBRE OPTIC SENSOR SYSTEM ON A MINE COUNTER-MEASURE VESSEL

5) NAMES OF AUTHOR(S) IN FULL (surname first)

PRAN Karianne, HAVSGÅRD Geir Bjarte, WANG Gunnar, JOHNSON Gregg, DANVER Bruce, VOHRA Sandeep

6) DISTRIBUTION STATEMENT

Approved for public release. Distribution unlimited. (Offentlig tilgjengelig)

7) INDEXING TERMS

IN ENGLISH:	IN NORWEGIAN:
a) fibre optic sensors	a) fiberoptiske sensorer
b) strain sensors	b) tøyningssensorer
c) fibre reinforced composites	c) fiberforsterkede kompositter
d) intelligent structures	d) intelligente strukturer
e)	e)

THESAURUS REFERENCE:

8) ABSTRACT

The report contains information on sensor placement on board as well as results of data analysis. The tests show that the fibre Bragg grating based sensor systems perform well and that the technology is suited for naval structure monitoring applications. We demonstrate the capability of monitoring the major dynamic load cases on this type of hull.

9) DATE	AUTHORIZED BY	POSITION
	This page only	
1 November 1999	Stian Løvold	Director of Research

ISBN-82-464-0383-4

UNCLASSIFIED

SECURITY CLASSIFICATION OF THIS PAGE (when data entered)

CONTENTS

FIELD TEST WITH A FIBRE OPTIC SENSOR SYSTEM ON A MINE COUNTER-MEASURE VESSEL

1 INTRODUCTION

This report describes the field test that was done under project “711 - Fiberoptisk skrogovervåkning” (CHESS) in April 1998. In this test 27 fibre optic strain sensors were installed on the Mine Counter Measure Vessel (MCMV) KNM Hinnøy, and measurements were recorded on several trips, both in the Haakonsvern area and on a trip to Kiel in Germany. The sensor system was expanded compared to an earlier test on this vessel **(1)**, and the sensor locations were better suited for recording hull flexure.

Both sensor elements and read-out electronics were provided by NRL, while the installation of sensors and cabling was performed by FFI staff in the course of three days. Personnel from both NRL and FFI took part in the measurement trips, and both institutions have copies of the full data set.

The sensor system and sensor locations are described, and some initial data analysis results are presented. We outline the further analyses that should be undertaken, and make suggestions for the final CHESS system based on the conclusions we can draw from these early analyses. The signal analysis presented in this report has been done at FFI.

Figure 1.1 KNM Hinnøy is an Oksøy class Mine Counter-Measure Vessel (MCMV)

2 SENSOR SYSTEMS

All sensors that were used were based on fibre Bragg gratings (FBGs) and they were interrogated using either of two readout techniques. One technique is the interferometric interrogation used in the previous CHESS field test, which is based on an unbalanced Mach-Zehnder interferometer. The other technique is based on a scanning Fabry-Perot filter.

2.1 Strain sensor system with interferometric interrogation

The strain sensor system with interferometric interrogation was a subsystem of the one used in previous experiments in the CHESS project (4). It was an eight-channel system with a combination of wavelength division multiplexing and spatial multiplexing, see Figure 2.1. A total of eight fibre Bragg gratings were divided between two arrays, with four gratings each. The light from each grating array was sent through a slightly unbalanced fibre Mach Zehnder interferometer in order to convert the wavelength changes induced by the strain into phase changes $\Delta\phi$ given by

$$\Delta\phi = -2\pi nd\frac{\Delta\lambda_b}{\lambda_b^2} = -2\pi nd\frac{1-p_e}{\lambda_b}\varepsilon, \qquad (2.1)$$

where n is the effective fibre index, d is the geometrical path imbalance, λ_b is the Bragg wavelength, $p_e = 0.22$ is the effective photoelastic constant and ε is the longitudinal strain. The optical path imbalance (nd) was for the "old" four-channel system 1.82 mm, and for the "new" four-channel system 1.7 mm. The channels were demultiplexed in the WDM filters, splitting the light into eight fibres, where each channel was detected and the phase retrieved using Phase Generated Carrier modulation and a Differentiate and Cross Multiply (DCM) demodulation technique (2). The PGC implies a high frequency modulation of the phase, which was done by applying voltage to a fibre-wrapped piezoelectric cylinder in one of the interferometer arms. The modulation was applied such that a tensile strain on the gratings led to a positive phase change in the output for both systems. Both the demodulated output and the quadrature (sine and cosine) signals were recorded during the tests.

The quadrature signals have been post-processed using an inverse trigonometric technique (3). This demodulation technique produces phase signals with frequencies from a few mHz to 7 kHz. The low frequency part is limited by drift in the interferometers, while the high frequency limit is given by the modulation frequency, which was 20 kHz. The DCM demodulators have a lower cut-off frequency on the order of 2 Hz, which makes them unsuitable for demodulation of low frequency signals. Since the frequency content in the strain signals is dominated by low frequencies, all the results from the interferometric system presented in this report have been processed using the inverse trigonometric technique.

As mentioned above, the frequency range of the interferometric interrogation system was from a few mHz to 7 kHz, but most of the collected data were recorded with a 2.5 kHz bandwidth. The noisefloor of the system was less than 10 $n\varepsilon/\sqrt{Hz}$ @ 1 kHz for all the channels, while the maximum strain value for these sensors was ±2300 με, due to the 5.5 nm bandwidth of the WDM filters used. Here it is assumed that the gratings have initial Bragg wavelengths in the passband centres.

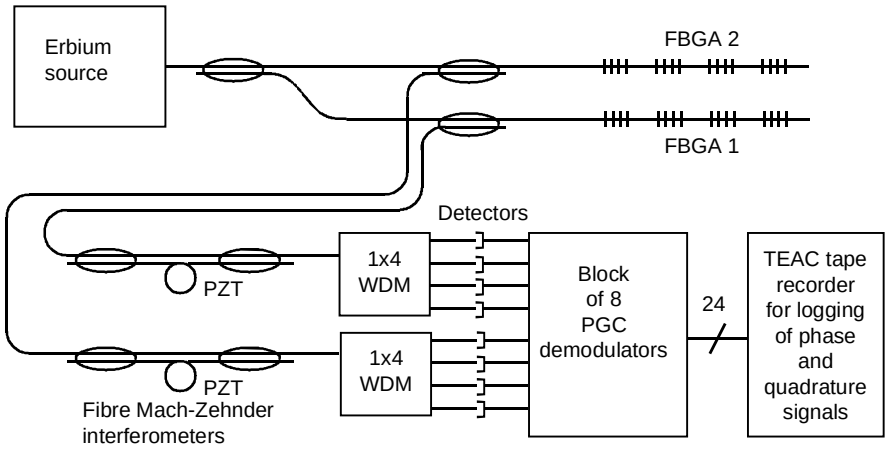

Figure 2.1 The Bragg grating strain sensor system with interferometric interrogation used in the sea test

2.2 Strain sensor system with scanning Fabry-Perot filter interrogation

The second interrogation system used in the sea test was based on a scanning fibre-optic Fabry-Perot filter. It was capable of interrogating four Bragg grating arrays, with up to 16 gratings in each array, using the optical configuration shown in Figure 2.2. The light source was a broadband source based on erbium doped fibre, and was filtered by the Fabry-Perot, which was made by Micron Optics. The filter had a free spectral range of about 40 nm, and a bandwidth of about 0.3 nm. After passing through the Fabry-Perot, the light was divided between four fibre Bragg grating arrays, and the light reflected from each array was detected by a separate photodiode.

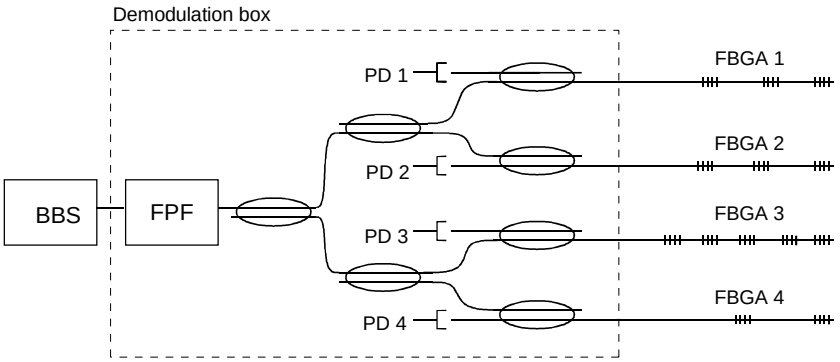

Figure 2.2 Optical configuration of the Fabry-Perot system used in the sea test. The light source is an erbium broadband source (BBS). The input light is filtered by the Fabry-Perot filter (FPF) and sent to four Bragg grating arrays (FBGA). The light returned from each array is detected at a separate photodiode (PD)

The passband of the Fabry-Perot filter was scanned through the wavelength region of interest, and a peak was detected every time a grating reflection wavelength coincides with the passband. The scan was triangular, with a frequency of 358.7 Hz, as shown in Figure 2.3. Two Bragg grating arrays (no 1 and 3) were interrogated during the scan towards longer wavelength, while two arrays (no 2 and 4) were interrogated on the scan towards shorter

wavelengths. The short flat periods at the top and bottom of the scan were used for communication with the PC that was controlling the system.

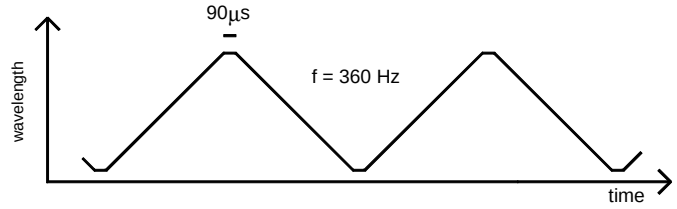

Figure 2.3 The Fabry-Perot filter was scanned using a triangular waveform

The shape of the detected peak is determined by the convolution between the Bragg grating spectrum and the filter spectrum. The peak is thus rather wide, and an exact determination of the centre is difficult. Therefore, the detected signal was differentiated, and the exact time of the zero-crossing for the differentiated signal was used to determine the Bragg wavelength.

In order to compensate for drift in the Fabry-Perot filter and for temperature drift of the Bragg wavelengths, one Bragg grating was strain isolated and used as wavelength reference for the system.

In addition to the optical components, the system consisted of analogue electronics for detection and amplification of the light and for zero-crossing detection. The system also contained digital electronics for generation of the triangular signal for the Fabry-Perot filter, and for communication with the PC, where the strain values were calculated. The PC used was a Compaq laptop with a Pentium processor.

The triangular signal was generated with 16-bit resolution. The zero-crossings were also detected with the same 16-bit resolution, which in a 40 nm range corresponds to a strain quantization of about 0.5 με. The actual noisefloor has not been measured, but measurements done during the sea test showed an rms noise value of about 1 με in a 90 Hz bandwidth.

As mentioned above, the scanning frequency of the Fabry-Perot filter was 358.7 Hz. This was also the maximum sampling frequency of the system. However, if only a lower bandwidth is needed, the effective sampling frequency can be reduced through averaging of a number of scans. This will also reduce the noise level in the measurements somewhat, but not unlimited, because of the quantization level. In the sea test, the measurements were done with either two or four averages, and thus an effective sampling rate of 179.35 or 89.67 Hz.

The data collected by the Fabry-Perot system were stored on the hard disk of the PC controlling the system. The data were stored in ASCII-format with array 1 first, then 2, 3 and 4. The individual channels were stored in the sequence that they were encountered by the Fabry-Perot filter, that is with increasing wavelength for array 1 and 3, and with decreasing wavelength for array 2 and 4. The data from the reference grating were stored in the first column in the files. Data could be stored in two modes; either manually or automatically. In the automatic mode, the system collected data for a certain amount of time if a selected channel reached a set threshold level (data were collected for all the channels). When the

saving was finished, the system started waiting for the strain level to exceed the threshold again. In the manual mode, data saving could be started and stopped by the operator at any time.

2.3 Fibre optic accelerometers with interferometric interrogation

The fibre optic accelerometers that were used in the test were also based on fibre Bragg gratings. The transducer design, shown in Figure 2.4, was made from two parallel plates of length 2.54 cm and width 0.63 cm, with a concentrated mass placed between them. The fibre Bragg grating is placed on the bottom side of the lower plate. The entire beam-mass-grating system was placed inside an aluminium box, with entry and exit holes for the optical fibre. A total of four different accelerometers were used in the tests, with three different masses M, at 2, 8 and 22 grams. The sensitivities and resonance frequencies were 2, 5.5, and 12.5 $\mu\varepsilon/g$ and 1, 0.5 and 0.3 kHz, respectively. We used one accelerometer with mass M = 2 g, two with M = 8 g and one with M = 22 g. The transducer design is further described by Todd et al (8).

The accelerometer Bragg wavelengths were read using the interferometric technique as described in section 2.1. The gratings were wavelength division multiplexed and four of the ports on the 1x8 WDM used in previous tests (4) were utilised together with a Mach-Zehnder interferometer with path imbalance, OPD = 2.38 mm. Both demodulated phase and quadrature signals were recorded on tape during the tests.

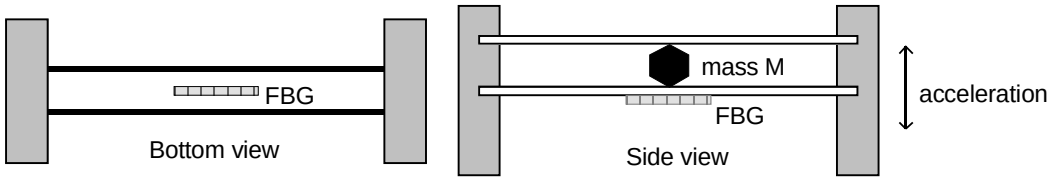

Figure 2.4 Schematic of the fibre optic accelerometers used

2.4 Installation of sensor system

From each sensor position a three-millimeter fibre optic cable was drawn along the ship's cable gates to the ship's office, located on the port side on deck 1. The cable was put through the watertight bulkheads using vacant spaces in the standard Brattberg throughputs.

The optical source, the readout electronics and optics and the tape recorders were all placed on a relatively small table in the ship's office, as shown in the picture below. Note that the same light-source was used for both all the systems, both strain sensors and accelerometers. This equipment can be reinstalled in a couple of hours in case we wish to make more measurements.

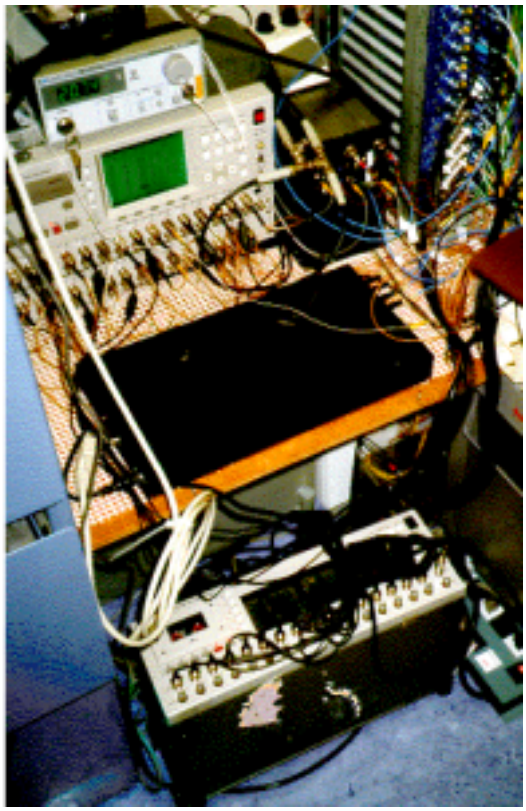

Figure 2.5 The readout and recording equipment was placed on a small table in the ship's office

3 SENSOR PLACEMENT

The strain sensors were grouped in six different arrays of which two were designed to be interrogated using an unbalanced Mach-Zehnder interferometer and the remaining four were interrogated with the scanning Fabry-Perot filter. The positions of the arrays and individual sensor elements are indicated in Figure 3.1. In addition we tested four FBG accelerometers that were placed on the wet deck. These were also interrogated interferometrically.

The sensor positions were chosen to enable monitoring of global flexures of the hull in addition to local strain concentrations in a limited number of locations. The basic global flexural modes are, with reference to the axes given in Figure 3.1, longitudinal bending in the xz-plane (sag/hog motion), longitudinal bending in the xy-plane (wagging), longitudinal compression, transverse bending, transverse compression and torsion about the x-axis. We expect the compressive modes to be weakly excited.

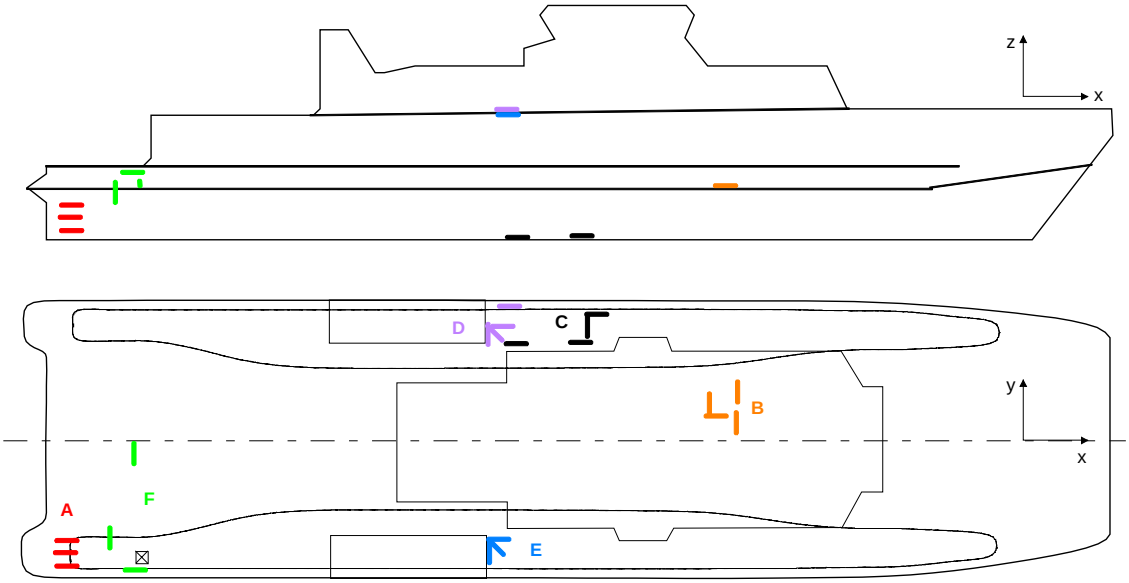

Figure 3.1 Locations of the six sensor arrays on KNM Hinnøy

Array A consists of four gratings with wavelengths that match the passbands of a 1x4 DWDM used with the Mach-Zehnder interferometer. These sensors were to measure the strains near the flange on the water jet tube, and they were placed approximately 8cm from the flange in continuance of four of the 24 bolts securing the tube. The positions are shown in Figure 3.2. These positions are inaccessible when the boat is in normal operation, and we chose to fix the grating elements to the tube surface with the 10-minute epoxy named Araldite 2010. The lead fibre was protected with a polyurethane adhesive, Araldite 2018.

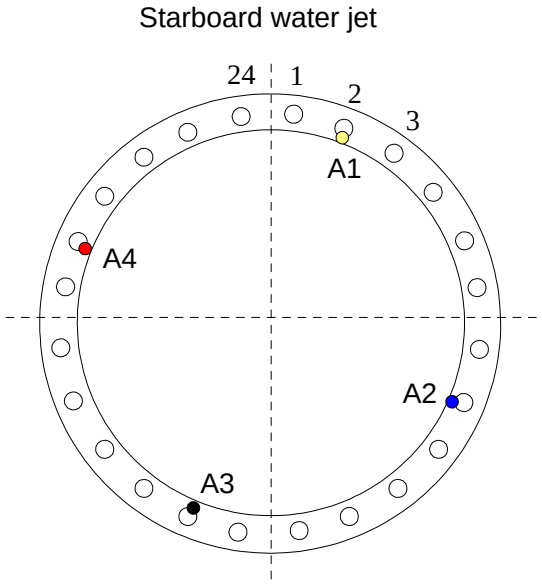

Figure 3.2 Array A; sensor positions with reference to the bolts in the flange of the water jet tube

Figure 3.3 From mounting of sensors on the water jet tube

The same adhesives were used to mount array B which is positioned on a wet deck panel near the sonar arm. This four-element array was installed in connection with the first CHESS field experiment in September 1996 (**1**), and can be interrogated with the Mach-Zehnder interferometer. We observed no significant changes in the properties of the array after the 1.5 year long exposure to conditions on board.

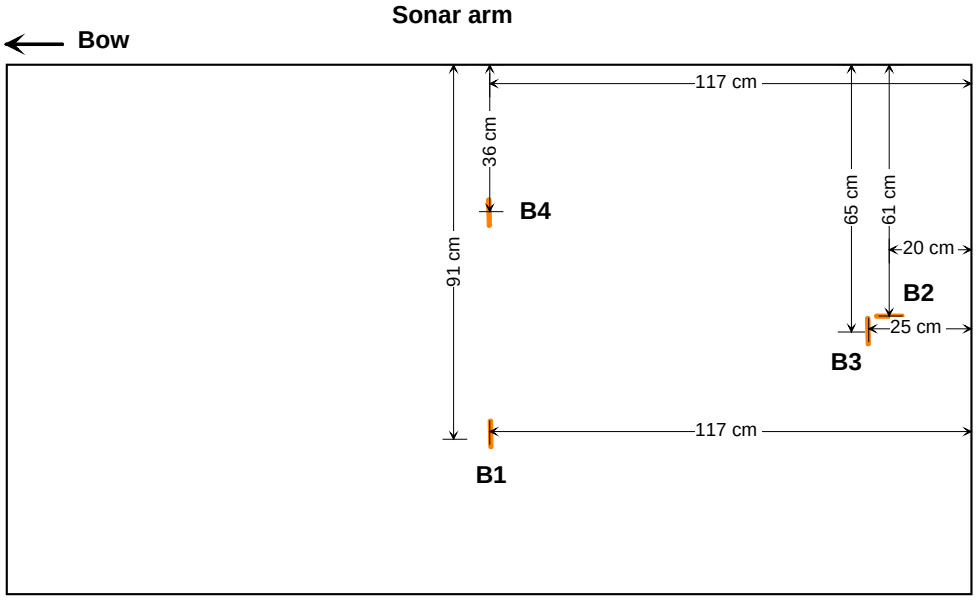

Figure 3.4 Sensor positions in array B with reference to the compartment walls on the wet deck

The interferometric interrogation technique was used for all the measurements on array B near Bergen and on the passage to Kiel, while during operations near Kiel and on the return from Kiel, the array was moved to the Fabry-Perot system. The detailed array layout is shown in Figure 3.4.

Array C is placed on a bottom panel amidships in the port side hull under the fan inlets. The six gratings in this array are shown in Figure 3.6. Sensor C1 is meant to measure mainly

global longitudinal bending together with grating D4, which is placed directly above C1 on deck. C1's position close to the panel edge at bulkhead 28600 should isolate it somewhat from the local panel vibrations.

The five remaining sensors C2-C6 are meant to monitor the panel vibrations and bending. The bottom panels are designed to be very flexible and this panel is not attached to bulkhead 24900 or to bulkhead 26100. This means that the alongships sensors in particular may see very high values of strain. All gratings were mounted using Araldite 2010. Since the sensors are placed in an area where they may occasionally be stepped on, the lead fibre was covered with woven glass fibre tape, which was then saturated with the epoxy SP106.

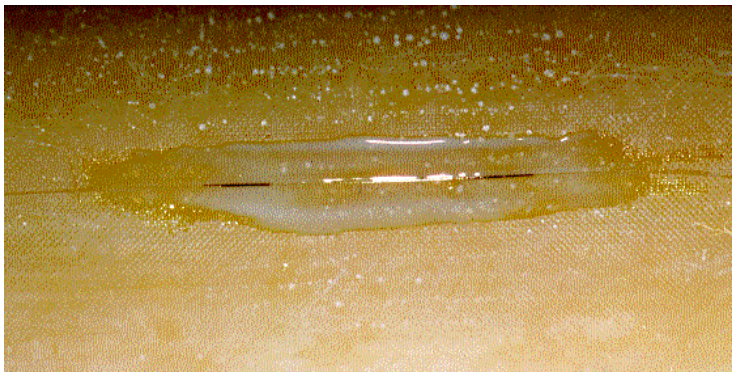

Figure 3.5 *A Bragg grating mounted with Araldite 2010. The fibre was afterwards protected with either polyurethane-based glue or with glass fibre tape saturated with epoxy*

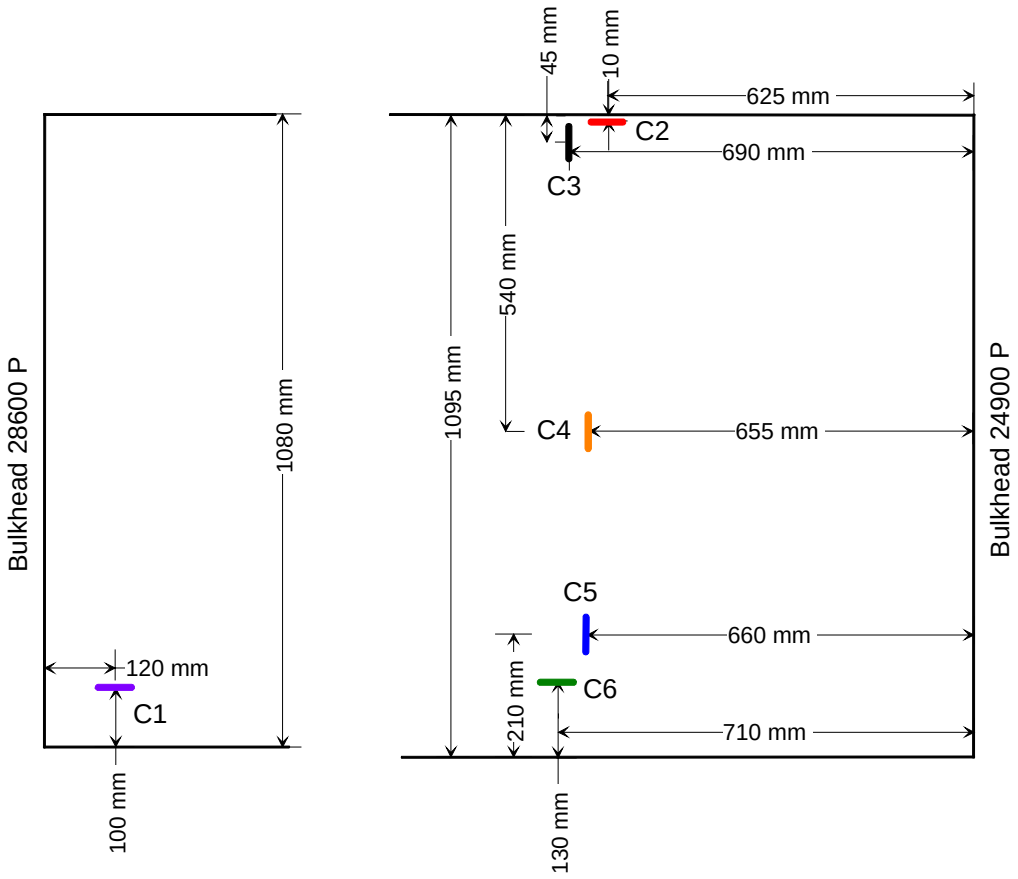

Figure 3.6 *Array C on the amidships bottom panel*

Arrays D and E are placed on the 01 deck in front of the casing on the port and starboard side respectively. They both contain a rosette that measures strain in three directions to fully characterise the strain condition at that point. The two rosettes together measure torsional bending of the hull. Array D also contains a fourth grating placed near the railing directly above sensor C1, and these two sensors measure longitudinal bending. The two arrays D and E are placed in a highly trafficked area of the deck and were covered with glass fibre tape and epoxy for protection. The sensor elements were attached with Araldite 2010. The detailed sensor positions are shown in Figure 3.7 and Figure 3.8.

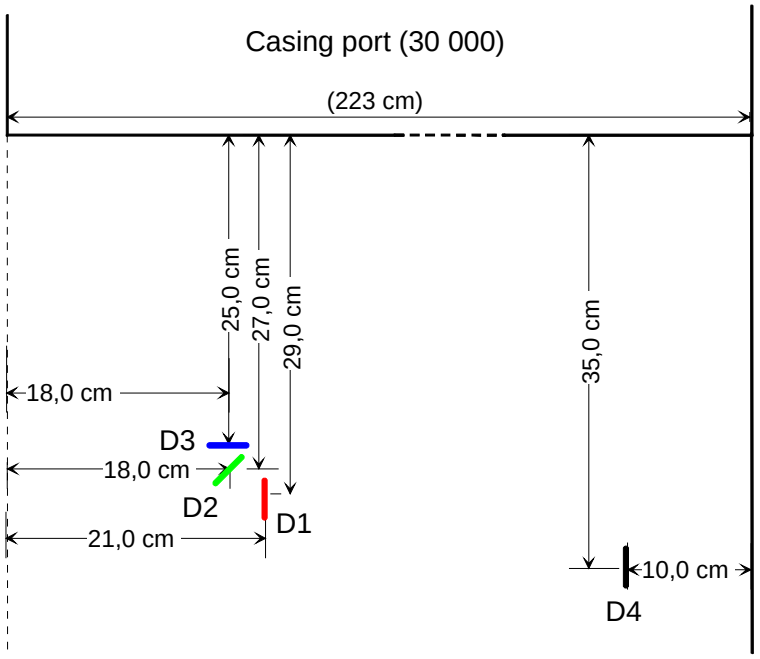

Figure 3.7 Array D mounted on deck 01 (port

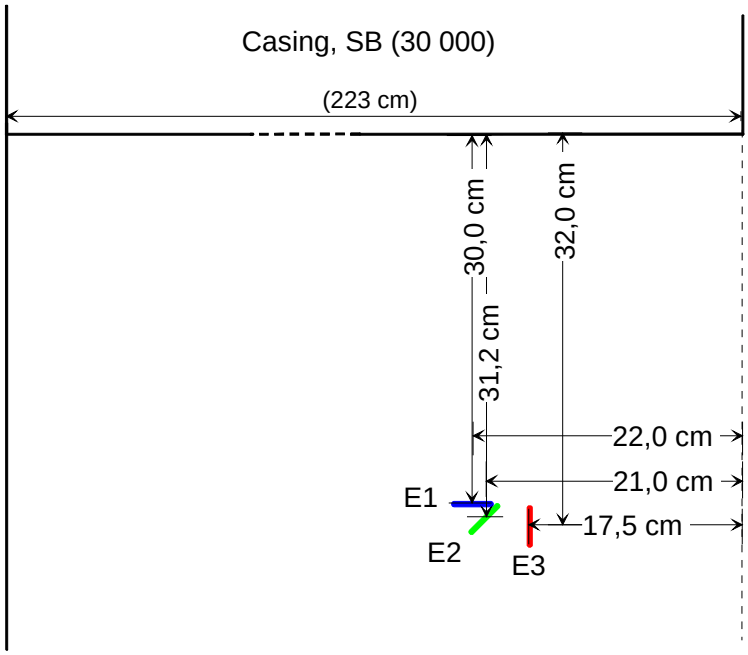

Figure 3.8 Array E mounted on deck 01 (starboard)

Array F is spread over a rather large area near the starboard water jet as sketched in Figure 3.9. It contains a strain-isolated reference grating (F1) that is used as a wavelength reference in the Fabry-Perot system. The next three gratings F2-F4 form a rosette measuring strain concentrations on bulkhead 48075 at the transition from the wet deck to the starboard side hull. Sensors F5 and F6 are placed on bulkhead 46700 near the centre axis of the boat and measure transverse bending. The final grating, F7, measures in the alongships direction and is placed in the compartment ceiling by the hatch leading down to the compartment from deck 1, 46cm astern of bulkhead 46700. The detailed positions of sensors F2 to F6 can be found in Appendix A.

Figure 3.9 Approximate positions of the seven sensors in array F, details in Appendix A

Information on the sensors that were interrogated with the Fabry-Perot system can be found in Table 3.1. The table lists the corresponding channel number and sensor identifier with a short description of the placement of that sensor and the Bragg wavelength

Channel	Sensor	Description	Wavelength (nm)
1	F1	Wavelength reference	1534.0
2	F2	Rosette 48075, horizontal	1538.0
3	F3	Rosette 48075, 45°	1541.83
4	F4	Rosette 48075, vertical	1545.82
5	F5	Transverse bending 46700, upper	1549.7
6	F6	Transverse bending 46700, lower	1553.8
7	F7	Local strain near hatch	1557.9
8	D1	Port rosette, alongships	1556.08
9	D2	Port rosette, 45°	1549.0
10	D3	Port rosette, abeam	1541.48
11	D4	Port casing, longitudinal bending	1533.65
12	C1	Port keel, longitudinal bending	1534.3
13	C2	Amidships panel, alongships upper position	1538.5
14	C3	Amidships panel, abeam upper position	1542.43
15	C4	Amidships panel, abeam middle position	1546.53
16	C5	Amidships panel, abeam lower position	1550.68
17	C6	Amidships panel, alongships lower position	1554.65
18	E1	Starboard rosette, abeam	1556.3
19	E2	Starboard rosette, 45°	1549.38
20	E3	Starboard rosette, alongships	1541.95
18*	B4	Wet deck, abeam	1555.56
19*	B3	Wet deck, abeam	1547.24
20*	B2	Wet deck, alongships	1540.39
21*	B1	Wet deck, abeam	1532.79

Table 3.1 Fabry-Perot channels, array B replaced array E in the Fabry-Perot system in the Kiel-area and on the return to Norway

A set of four accelerometers was also used. This was interrogated using the Mach-Zehnder system, and the accelerometers were placed on the wet deck close to array B. Their relative positions are shown in Figure 3.10.

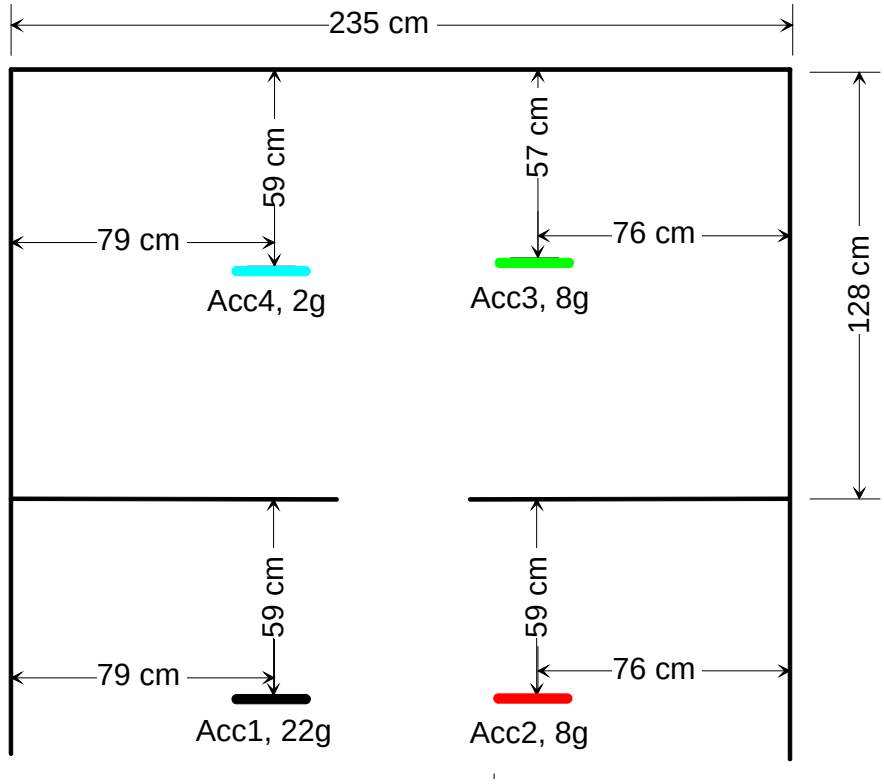

Figure 3.10 Accelerometer positions and masses

4 TEST PROGRAM

The sea test was divided into two parts, where the first took place in the fjords outside Bergen on April 1 and 2, 1998. The second part was on a transit from Bergen to Kiel April 18 and 19. Some data was also collected during the stay in the Kiel area, and some on the way back on April 27. In the description below, the hour is included for reference to the data sets that were collected.

4.1 Outside Bergen on April 1 and 2

On April 1, the test consisted of a trip from Haakonsvern to Marstein lighthouse and back. We left the quay at 10.30 am and returned at 2 pm. The conditions were relatively calm throughout the whole day, but the conditions were slightly rougher close to the lighthouse at around noon, and the sea-state was estimated to SS1. On the way back and forth the speed of the boat was about 20 knots, but the speed was reduced when near harbour. Close to the lighthouse, the boat went in circles for a while, in order to induce some strain in the hull.

On April 1 we were collecting data from a total of 24 fibre Bragg grating strain sensors and from the four accelerometers. The grating arrays were configured as listed in Table 4.1, except for array E, which had not been mounted yet, so that Fabry-Perot array 4 was not used.

Interrogation system	Bragg grating array
Fabry-Perot array 1	F (by waterjet)
Fabry-Perot array 2	D (on deck, port side)
Fabry-Perot array	C (under air cushion fans)
Fabry-Perot array	E (on deck, starboard side)
Interferometric array 1 (“old”)	B (on wet deck)
Interferometric array 1 (“new”)	A (on waterjet)
Interferometric array 1 (“8 ch”)	Accelerometers

Table 4.1 Channel configuration used on April 2 and on the transit to Kiel. On April 1, the configuration was similar except that array E was not used

On April 2, there was a new trip in the area outside Haakonsvern. This day was even calmer, and the strain levels were correspondingly low. The trip lasted for about four hours, starting at 10 am and finishing at 2 pm. The channel configuration was as listed in Table 4.1, now with a total of 27 strain sensor gratings and four accelerometers being interrogated.

On April 1, an effective sampling rate of 179.35 Hz was used for the Fabry-Perot system, but on April 2, the sampling rate was reduced to 89.67 Hz. We have approximately two hours worth of data from the Fabry-Perot system from April 1 and 2. The data from the interferometric system was collected continuously throughout the trips in a 10 kHz bandwidth on the TEAC tape recorder.

4.2 Transit to Kiel

The transit from Haakonsvern to Kiel took place from April 18 at 9 am to April 19 at 2 pm. The conditions were again very calm for the first part of the transit along the coast of Norway. From about 10 pm on April 18 to about 5 am on April 19, the conditions got slightly rougher across Skagerrak, and we experienced some movement of the boat, with the largest signals probably around midnight. The sea-state was estimated to SS1. We did, however, consider the conditions to be slightly rougher than outside Bergen on April 1. From 5 am to arrival in Kiel, the conditions were again extremely quiet, and no significant strain could be seen. The speed of the boat was about 20 knots throughout the transit.

The channel configuration was again as shown in Table 4.1. The Fabry-Perot system had an effective sampling frequency of 89.67 Hz, while the data from the interferometric system were collected in a 2.5 kHz bandwidth. We have about two hours of Fabry-Perot data on file, while data from the interferometric system was collected almost continuously.

4.3 In the Kiel area and transit to Mandal

For the test done in the Kiel area during the exercise and the on the transit back to Norway, only the Fabry-Perot system was used. The system was set up in the autosave mode, and was operated by the crew on KNM Hinnøy. The channel configuration was as listed in Table 4.2. We chose to remove array E (the starboard array on the 01 deck) and to interrogate array B (on the wet-deck). The effective sampling rate was again 89.67 Hz.

Interrogation system	Bragg grating array
Fabry-Perot array 1	F (by waterjet)
Fabry-Perot array 2	D (on deck, port side)
Fabry-Perot array	C (under air cushion fans)
Fabry-Perot array	B (on wet deck)

Table 4.2 Channel configuration used on April 23 and April 26. Note that the starboard rosette is removed and the wet-deck array (B) is installed

Some data were collected on April 23, during the exercise. The conditions were still relatively calm, and the boat was operating as a minesweeper. This means that the boat was operating at low speed (0-3 knots), and was going in circles part of the time, thus changing direction with respect to the waves quite rapidly.

The rest of the data set was collected on April 26, across Skagerrak on the way from Kiel to Mandal. The conditions were slightly rougher than before, with sea-state estimated to SS2. The boat was going at a speed of 20 knots. On this transit, the boat's bow-thrusters were not working, but this should not have any effect on the strain patterns in the hull.

We have about 12 minutes worth of data from the Kiel area, and about two hours from the trip back to Mandal.

5 INITIAL SIGNAL ANALYSIS

New information on the behaviour of the boat has been gained compared to the September - 96 measurements through the added sensor locations and the low-frequency response of the Fabry-Perot system. We will in the following try to illustrate some features of the recorded data with example excerpts, and at the same time we will describe the typical properties of the data from each sensor.

We have browsed though a significant part of the recorded data, and have picked out examples of behaviour for the different sensors. Some we have analysed further, in particular the sensors that measure longitudinal and transverse bending.

5.1 Examination of noise components

On April 1 a six-minute recording of data was made before the machinery was started. At that time all other systems were in operation, e g the ventilation. This chapter shows some examples of power spectra for different sensor locations and a compilation of the spectral components that are present in each sensor's spectrum.

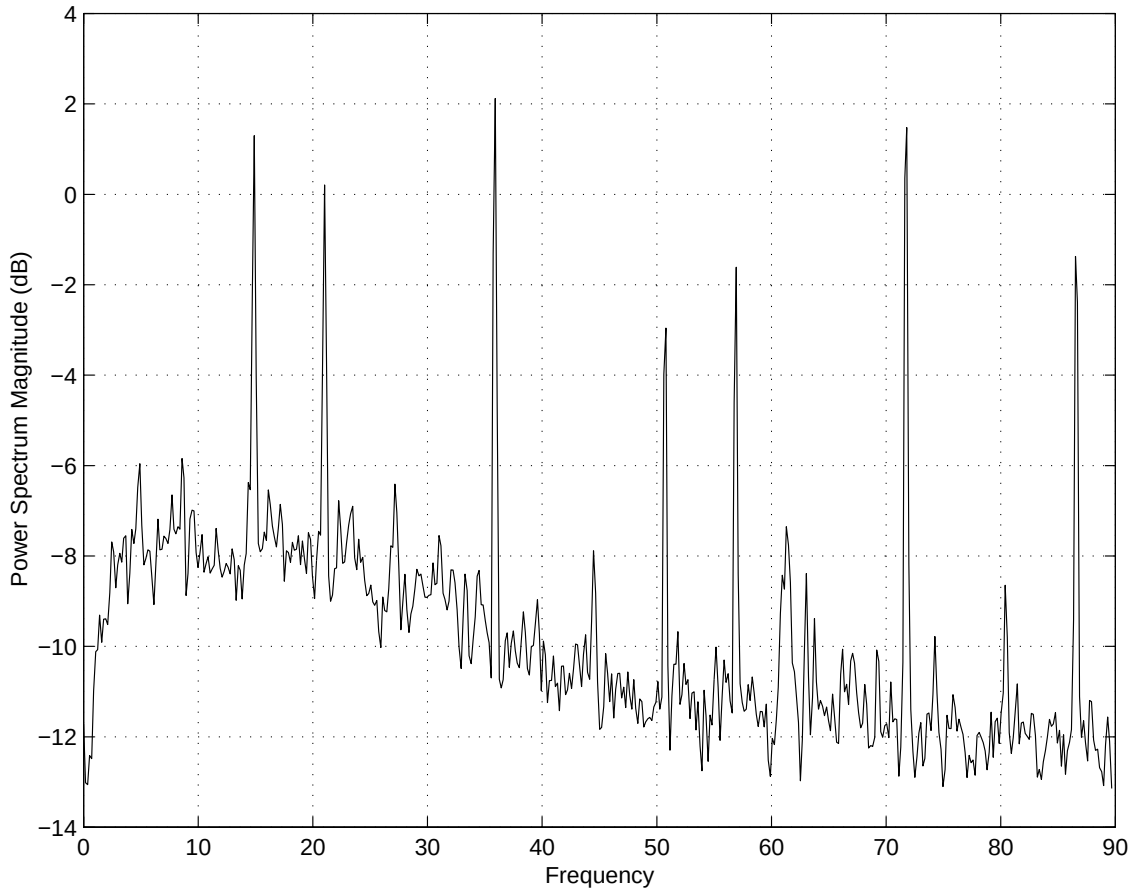

Figure 5.1 Power spectral density for the strain isolated reference grating

In Figure 5.1 we see that although the wavelength reference grating was not in contact with the hull its spectrum still contains a series of spectral components. The distinguishing feature of this spectrum is the lack of low frequency components. The main peaks are at 14.8, 21.0, 35.9, 50.7, 56.9, 71.7 and 86.6Hz.

Figure 5.2 shows the signal excerpt that has been analysed, together with the power spectral density for sensor F3, the 45° sensor in the rosette on bulkhead 48075. We see that the signal variance is in the ±2με region, and that the signal is dominated by low frequencies. Turning to the spectrum we find that the dominating component is at 0.3Hz with additional components at 0.5Hz and 2.5Hz. Comparing the higher frequency components with those of the reference we recognise most of them. The only addition is the component at 30Hz. The noise floor seems to drop above 45Hz, and this is more pronounced in the spectra for sensors F2 and F4 (not shown).

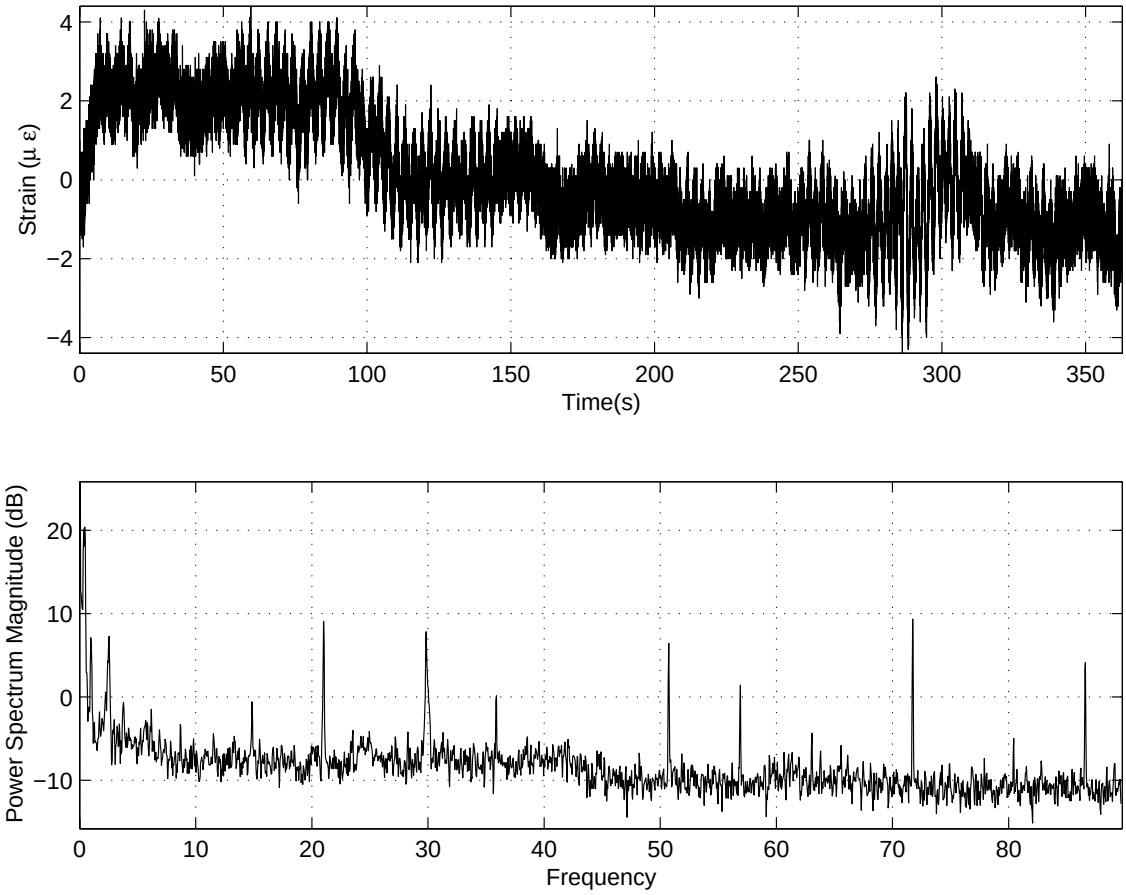

Figure 5.2 Time series (top) and power spectral density for sensor F3, 45° component of rosette on bulkhead 48075

Sensor C1 is placed on the bottom panel amidships, a position not unlike that of the along-ships sensor used in September -96. As expected from that earlier experiment we see a large component at 2.1Hz in Figure 5.3. At even lower frequencies we have components at 0.2 and 0.5Hz. In addition to the frequency components common to all sensors at 14.8, 21.0, 35.9, 50.7, 56.9, 71.7 and 86.6Hz, C1's spectrum has a peak at 45.5Hz.

This sensor is interrogated simultaneously with the reference. If we subtract the reference time series from that of C1 and find the spectrum of the difference we see in Figure 5.4 that the common frequency components disappear. This strategy is not as successful for the other channels, shown for example in Figure 5.5 where we have subtracted the reference from the signal of sensor C3 which is sampled at a later point in the Fabry-Perot scan cycle. The change in each part of the spectrum will depend on the phase change for that component between the time of sampling for the reference and the sensor in question.

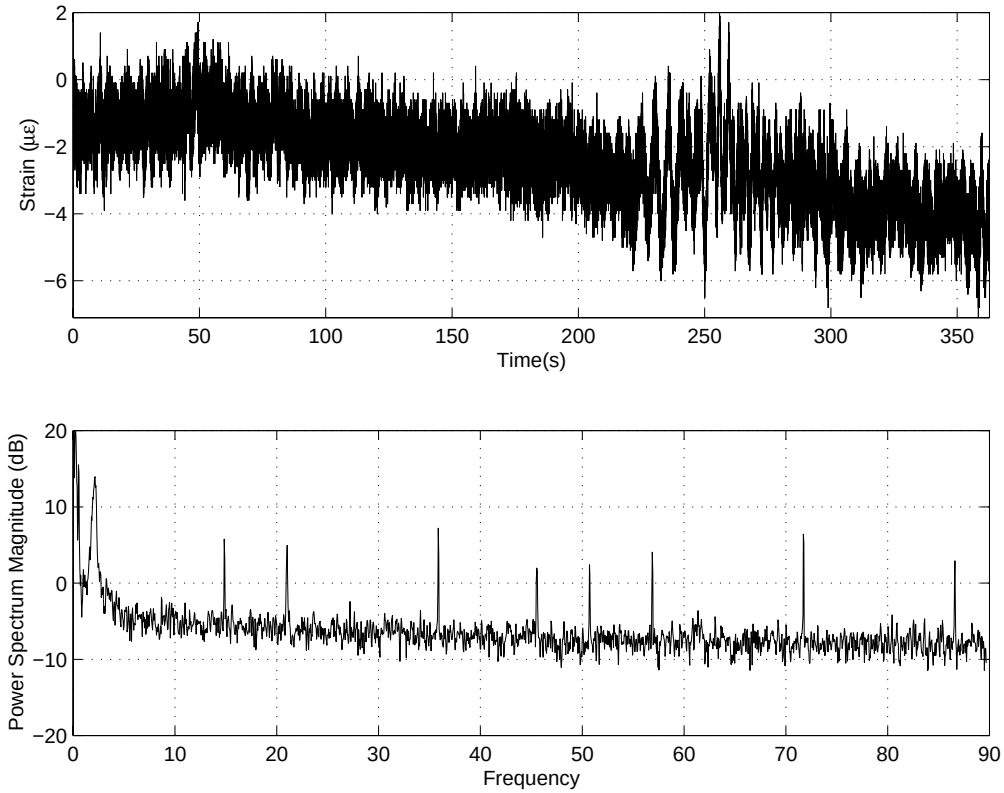

Figure 5.3 Time series and power spectral density for sensor C1, measuring long-ship at port keel

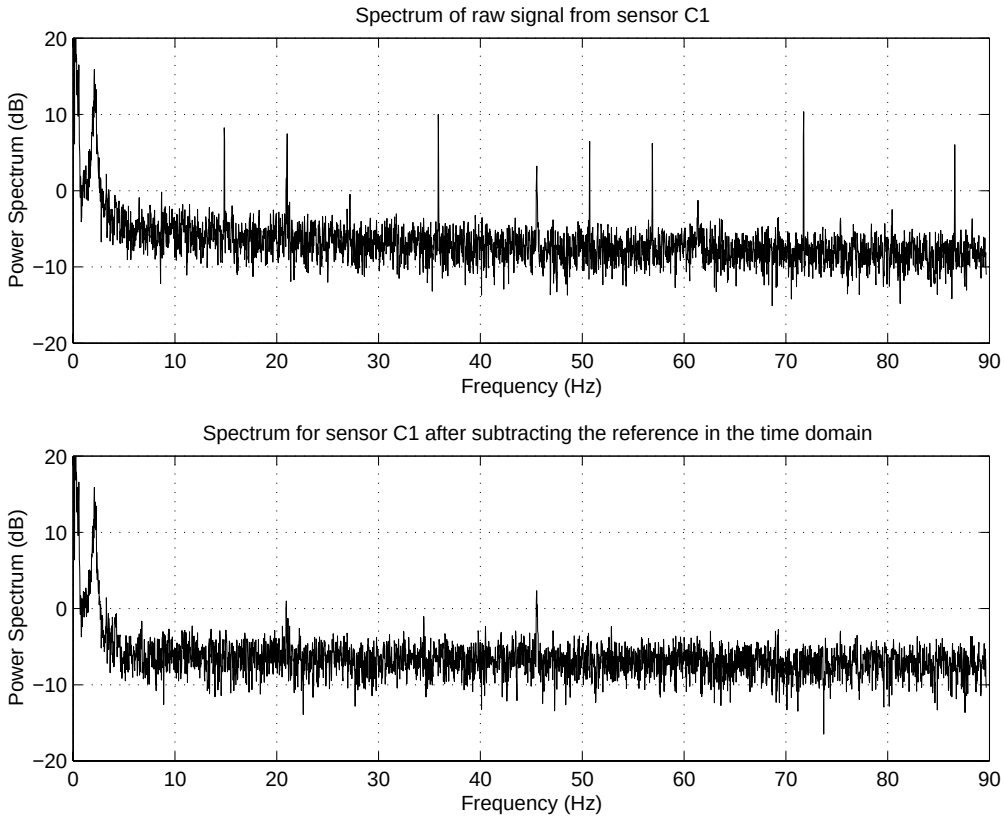

Figure 5.4 Power spectral density for sensor C1 before and after subtraction of the reference time series

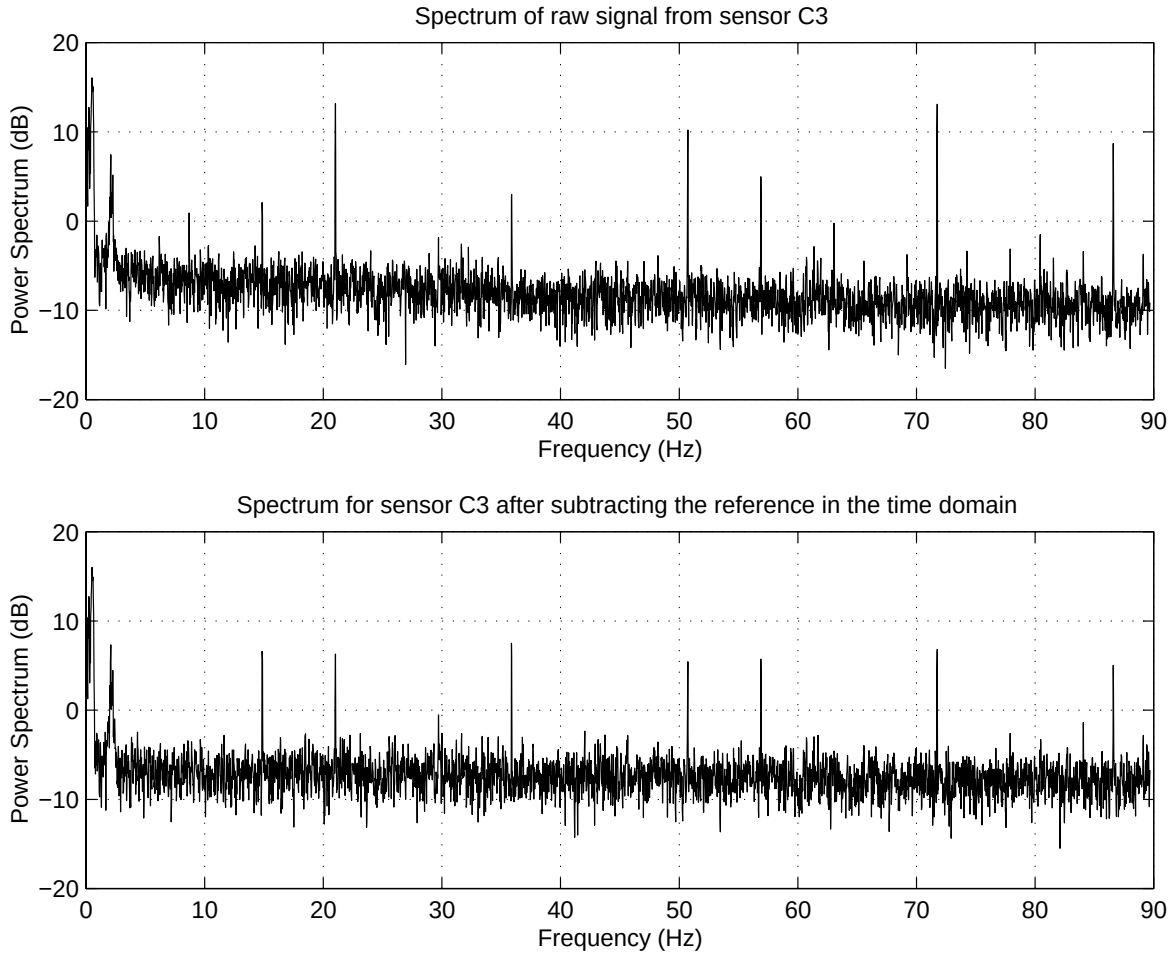

Figure 5.5 Power spectral density for sensor C3 before and after subtraction of the reference time series

There are two possible sources for this kind of noise. The frequencies can be generated by the Fabry-Perot system or they can represent acoustic noise picked up by the reference grating. The data stored for the reference grating is the measured strain, which is then used to generate the compensation signal. Since the noise is to some extent removable by subtraction of the reference it must be in phase in the different channels, and this indicates that the noise source is internal to the Fabry-Perot system, either in the scanning filter itself or in the read-out electronics. External noise in the reference would have been transferred to the other channels in opposite phase.

5.2 Excerpts from the Fabry-Perot system

The data sets recorded with the Fabry-Perot system the first hours after the ship left harbour shows large, relatively linear, strain changes. We have attributed this to temperature changes in the compartments containing machinery, and increased outside air temperature. In addition it takes some time for the Fabry-Perot system to reach a stable state. The background components seem to stabilise after some time.

In Figure 5.6 we have plotted 25 minutes of data from the two sensors F5 and F6. We see that the static strain level of F5 and F6 is constant. This should indicate that the system has

reached a stable state. Although constant, the static strain level may be different from zero since the strain level was set to zero at the beginning of every recording session with the Fabry-Perot system.

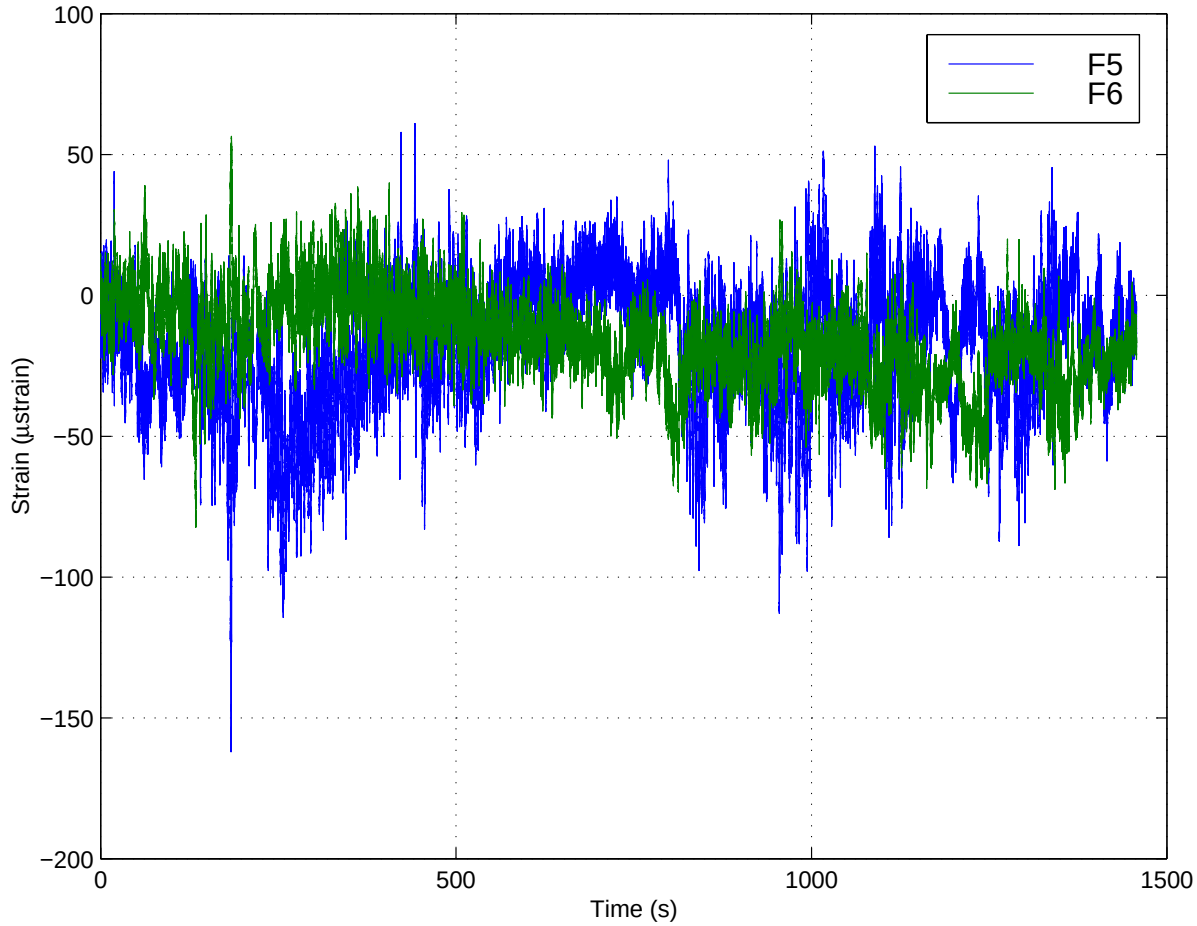

Figure 5.6 25 minutes of data for sensors F5 and F6 in approximately SS1 outside Bergen

In Figure 5.7 the same 25 minute excerpt is shown for the two alongships sensors D4 and C1. We see large variations in static strain levels, and these variations are probably due to real strain variations in the hull since they appear in both sensors. Unfortunately there is no record available on the boat's heading relative to the waves during this period.

It is typical for the whole experiment that the signals from D4 and C1 measuring longitudinal bending are very closely correlated, while there is not the same close relation between F5 and F6 which are meant to measure transverse bending.

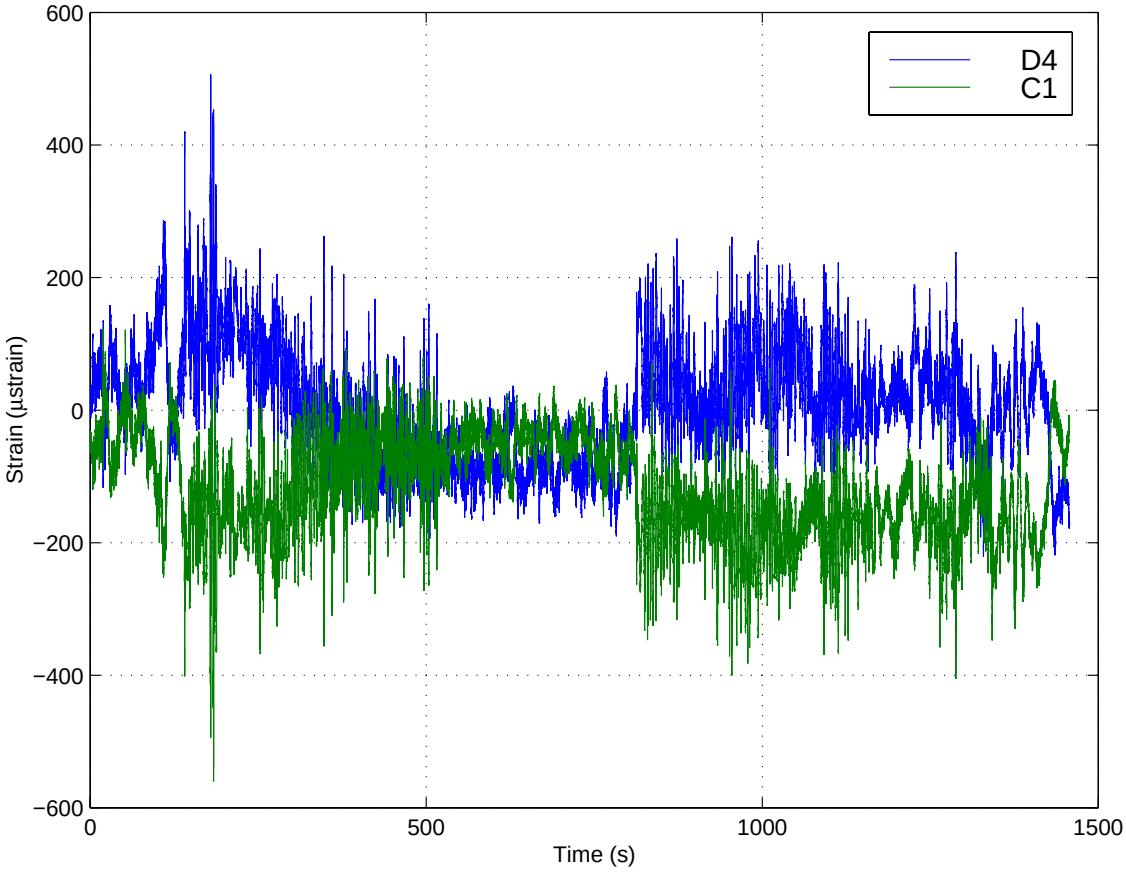

Figure 5.7 25 minutes of data for sensors D4 and C1 in approximately SS1 outside Bergen

In Figure 5.8 we have zoomed in on the curves for F5 and F6 to see the fine features. We notice that a main oscillation is transient in nature and has a frequency of 6-7Hz. The two signals are 180° out of phase, indicating transverse bending. The signals from F5 are more complex and have higher amplitudes. We see for instance a 2Hz transient in F5 that is not prominent in F6.

We expect some correlation between F5/F6 and the rosette placed at the transition from wet deck to starboard side hull since the exciting force of a transverse bending mode must be exerted on the keels of the two hulls. A signal excerpt for the rosette F2-F4 is shown in Figure 5.9. We recognise the 6-7Hz transient occurring at about 71.5s. The dominating oscillation seen in F2 is the 10Hz frequency of the water jet. An effort is being made in order to interpret the signals from rosettes, which will be presented in a separate report.

Next we have collected data from all the sensors that primarily measure longitudinal bending, namely sensors D4, C1, C2 and C6. Figure 5.10 shows that all four sequences are closely correlated as they measure bending due to wave-hull interaction at about 0.3Hz and bending due to excitation of the longitudinal bending mode at 2.4Hz.

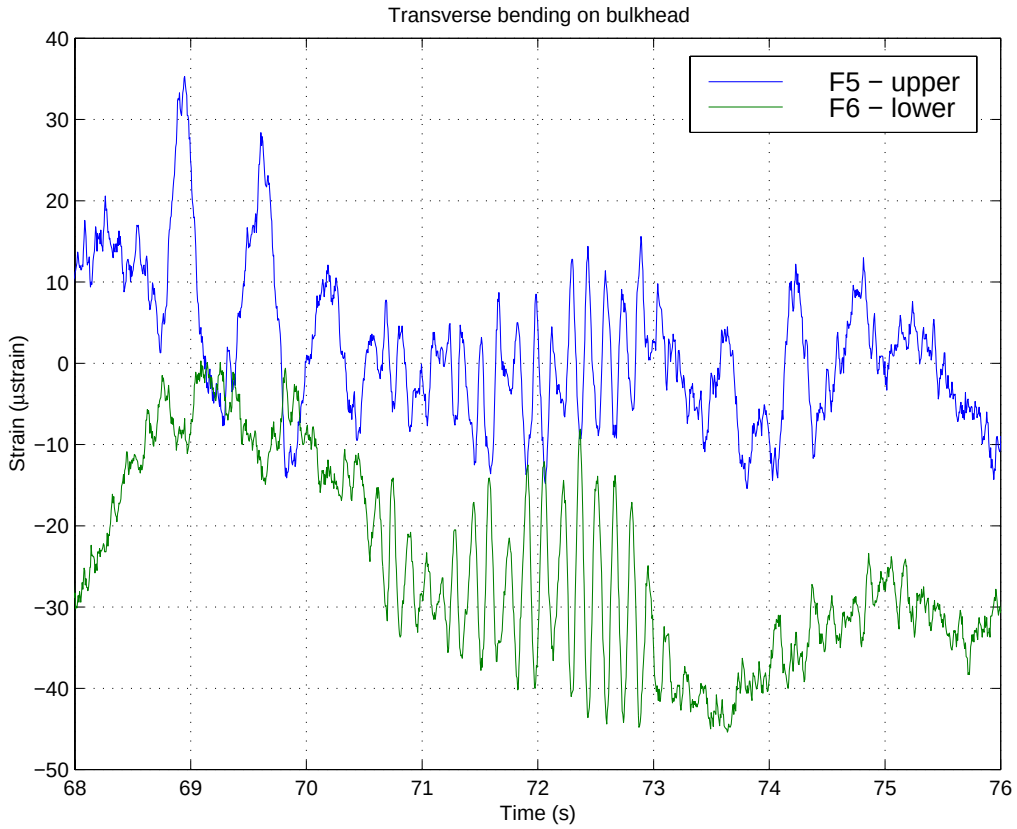

Figure 5.8 Excerpt from sensors F5 and F6 measuring cross-ship on bulkhead 47600

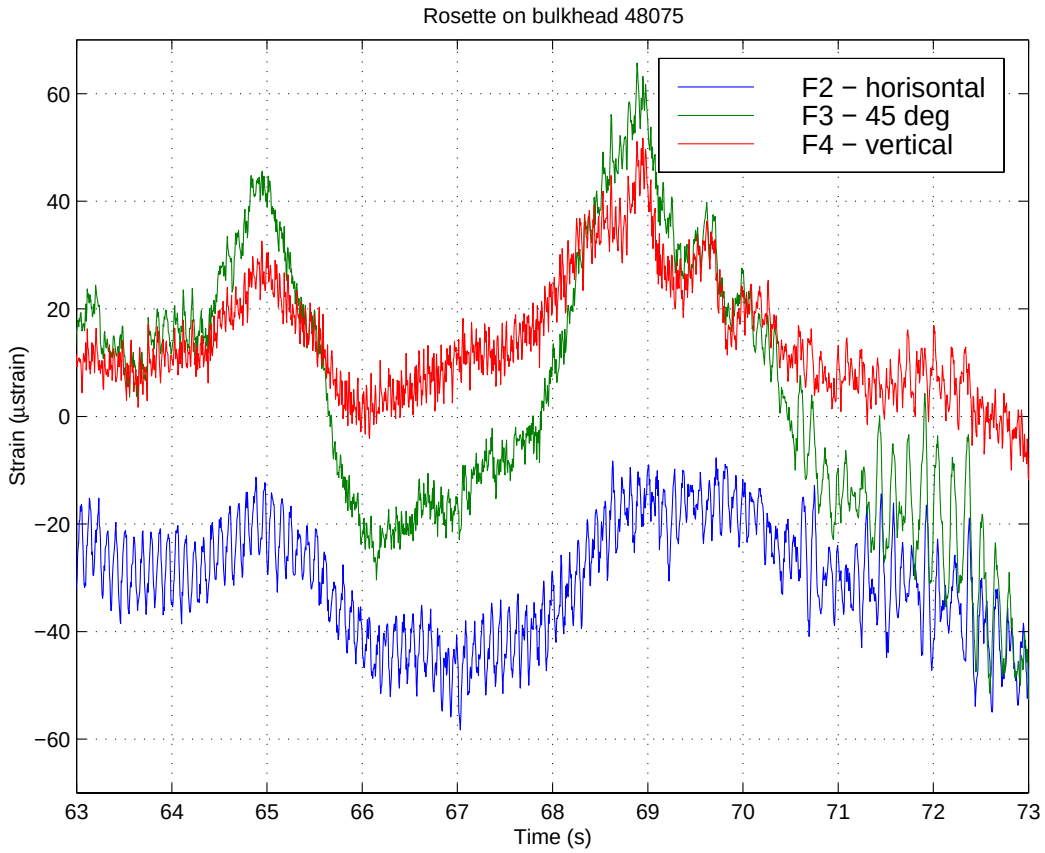

Figure 5.9 Excerpt from sensors F2, F3 and F4 forming a rosette on bulkhead 48075

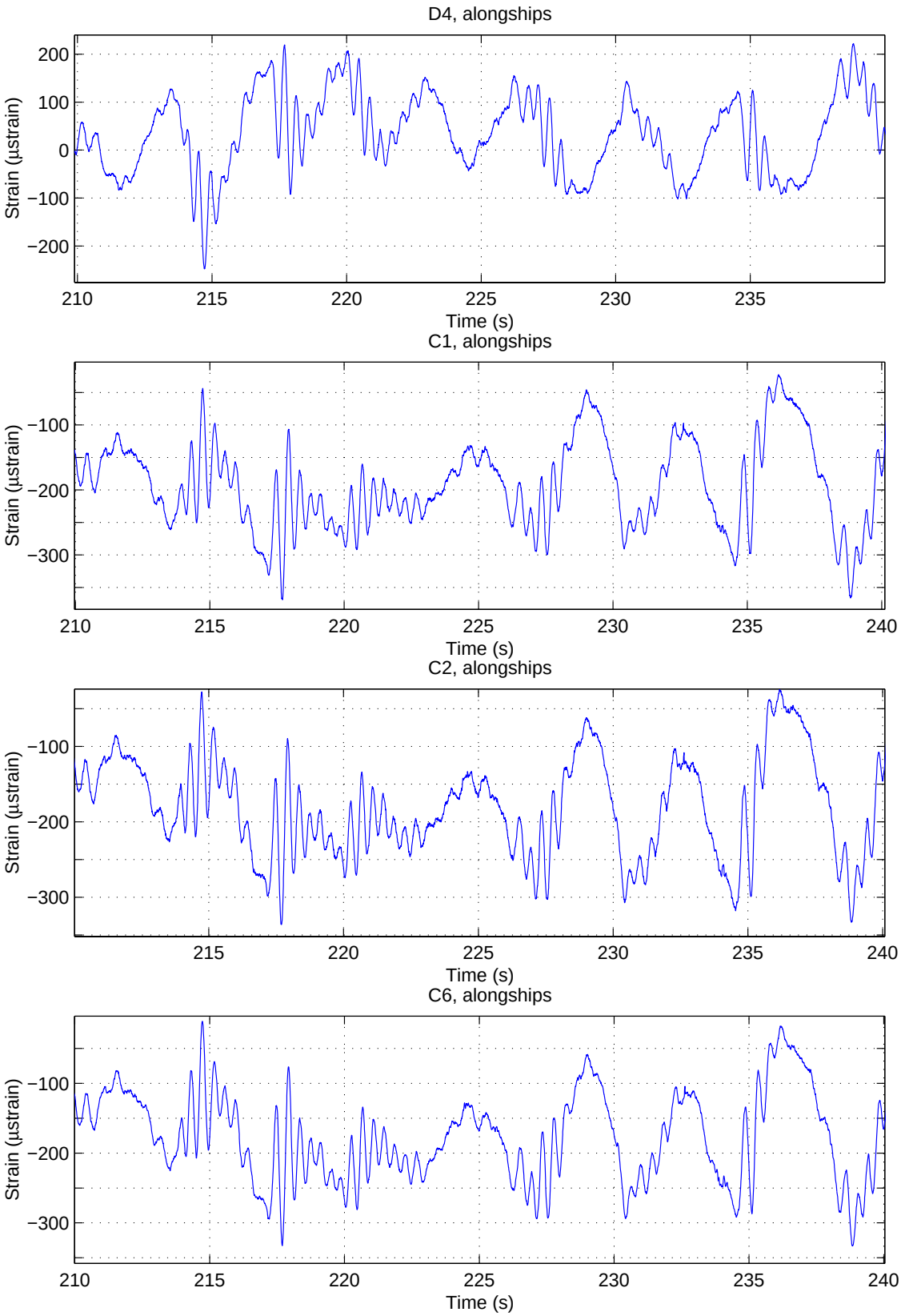

Figure 5.10 Long-ship bending in port side-hull; sensors D4, C1, C2 and C6

Although C2 and C6 are placed approximately 3m from D4/C1, there is no evidence that they measure other modes than D4/C1, eg a second order bending mode which would have a node amidships at D4/C1.

We have taken the Gabor transform of a signal sequence from C1 as shown in Figure 5.11. The logarithmic colour scale shows the almost continuous excitation of the 2.4Hz bending mode and the high energies at low frequencies due to wave-hull interaction. We also see transient events occurring at approximately 4.5Hz and 8Hz. In addition we clearly see the noise components at 21.0Hz, 50.7Hz, 71.7Hz and 86.6Hz. The continuous frequency components at 10Hz, 20Hz, 30Hz and 40Hz are consistent with the fundamental and higher harmonics of the water jet turbine. The waterjet and noise components are less prominent in higher sea-states.

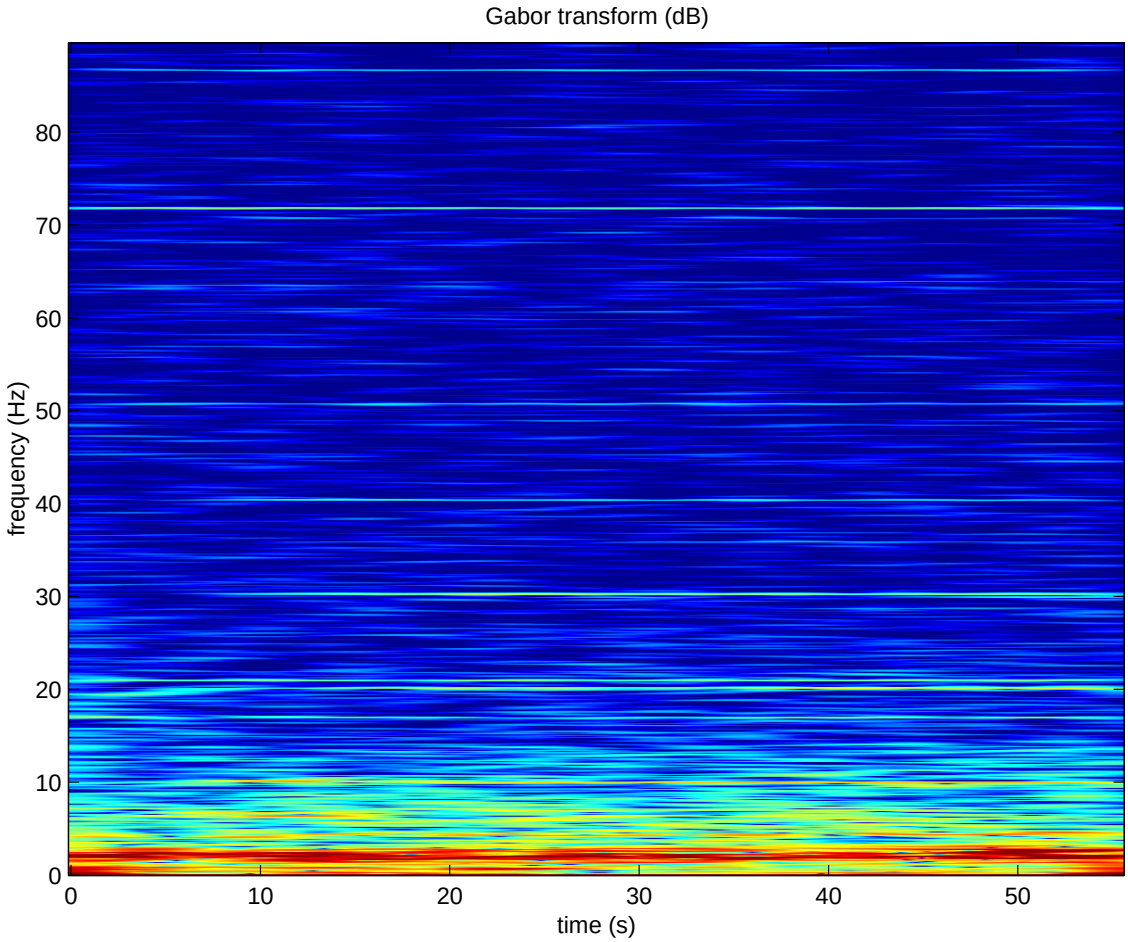

Figure 5.11 Gabor transform of the signal from sensor C1 measuring long-ship near the keel during low sea-state sailing

The three sensors C3-C5 all measure in the cross-ship direction on a bottom panel in the port side hull. A three-second excerpt is shown in Figure 5.12. The three signals are strongly correlated, but we see some higher frequency oscillations in the signal from sensor C4. This sensor is placed in the plate centre, and will consequently measure local panel vibrations that are not noticeable in the two sensors placed near the panel perimeter. The panel vibration is in the region 16-20Hz. We have seen very few instances of this panel vibration in the analysed data sets, and we think that the wave impacts in low sea-states are not hard enough to excite the vibration.

The panel vibration is superposed on a 2.4Hz component. This is the modal frequency for longitudinal bending, which is transferred to the cross-ship direction via Poisson's ratio. The source of the 10Hz transient occurring at 269.5s is as yet unidentified.

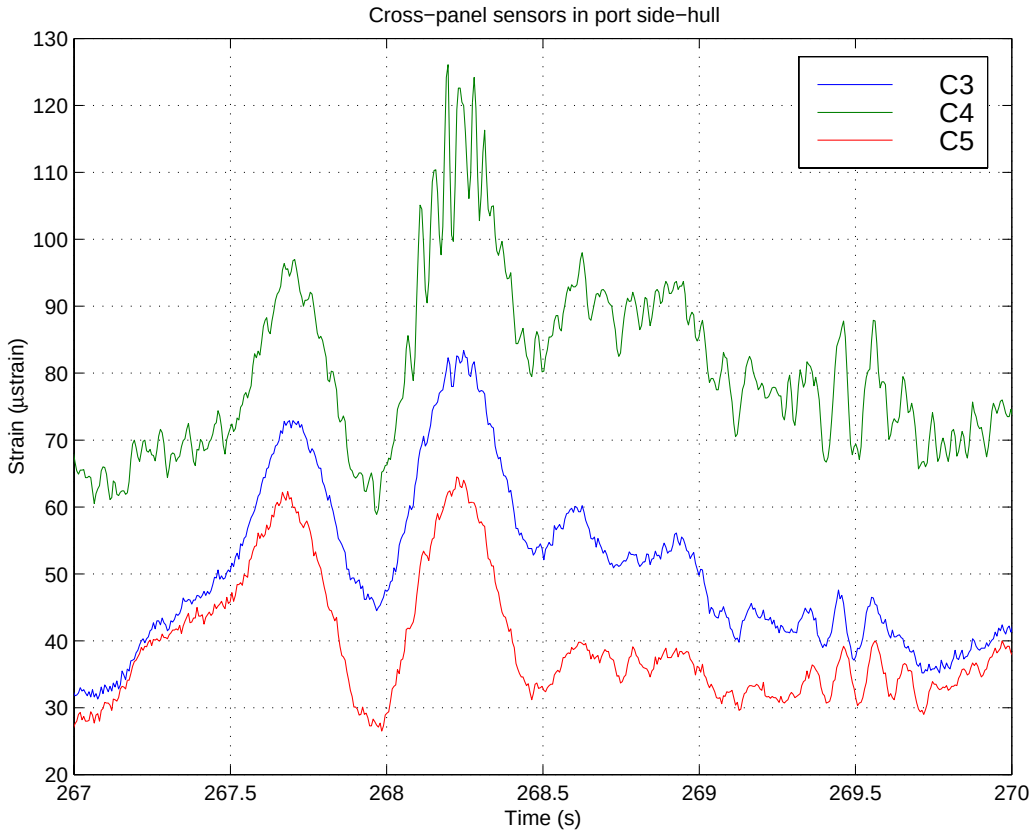

Figure 5.12 Cross-ship panel bending and vibration in port side-hull

Turning next to the rosette on the port side of the deck in Figure 5.13, we see a typical situation where D1 measuring in the longitudinal direction has the higher amplitude, with D3 closely correlated and 180° out of phase. The 45° sensor D2 will then measure the projection of D1 and D3 onto its own measuring direction, with a resultant lower amplitude oscillating in phase with D1. D1 and D3 are fairly closely correlated to the signals from D4, but their location is such that they also pick up local strain concentrations du to the casing. Surprisingly, D2 shows very low correlation with the other sensors during large parts of the data set, and also very low amplitudes. This has made us suspect that there is a problem with the adhesion to the hull for this sensor.

We have this far been unable to identify any likely frequency for the torsional mode that we anticipate, and which would have its main strain component in the direction of D2. Data from the rosette in array E is similar to measurements with D1 and D3. A signal excerpt from F7 is shown in Figure 5.14 together with a power spectrum. The sensor was mounted in a location where local strain concentrations were expected, and which is incidentally in a rather noisy part of the boat. This leads to the dense power spectrum for this signal sequence. Although F7 is mounted in the longitudinal direction it is very different from the other longitudinal measurements.

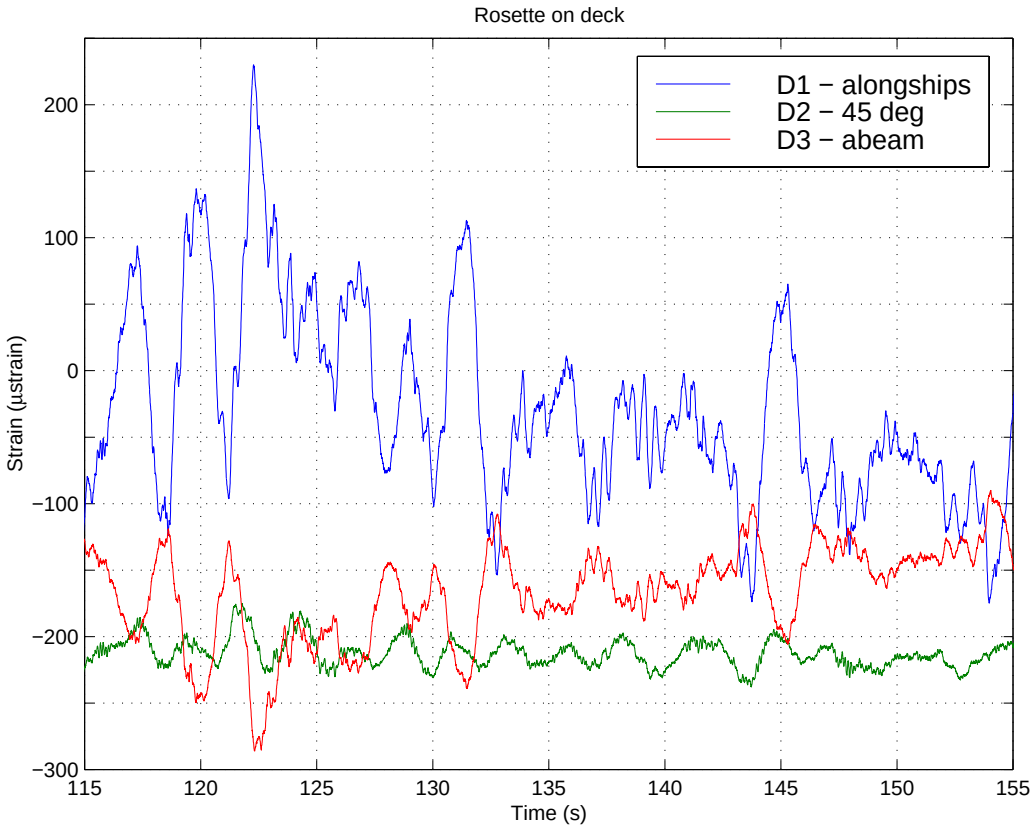

Figure 5.13 Rosette on deck, port side, sensors D1, D2 and D3

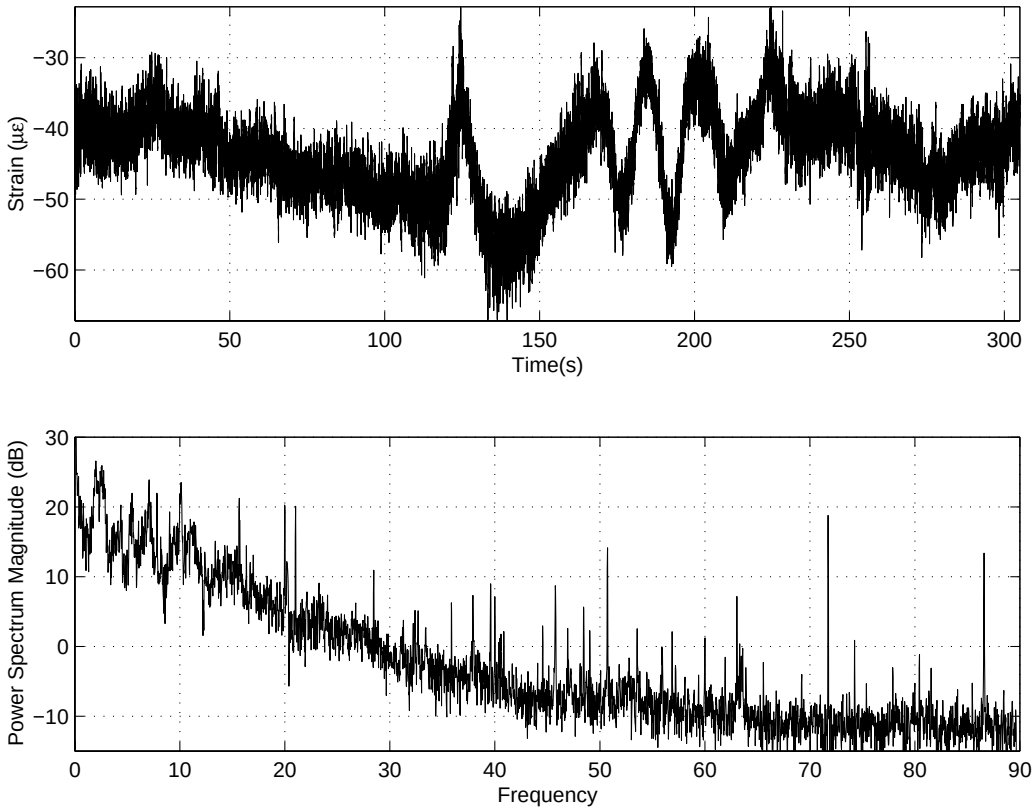

Figure 5.14 Time series (top) and power spectral density for sensor F7 measuring local strains near hatch under low sea state sailing

5.3 Excerpts with interferometric interrogation

The data from the Mach-Zehnder system, ie array A, B and the accelerometers were stored on tape and were subsequently sampled and transferred to file. The data sets used in this report were sampled at 200Hz for arrays A and B, and at 4kHz for the accelerometers.

Figure 5.15 shows a particularly eventful excerpt from array A on the waterjet. We see quasi-static strain changes of almost 600μstrain, and transients at 10Hz with amplitudes of about 180μstrain. This is not a typical situation. For the most part strain levels have been fairly constant with amplitudes at frequencies above 10Hz in the range 10-30μstrain. We notice from the figure that the higher loads are experienced by sensors A2 an A4, and this indicates horizontal rather than vertical movement of the waterjet tube.

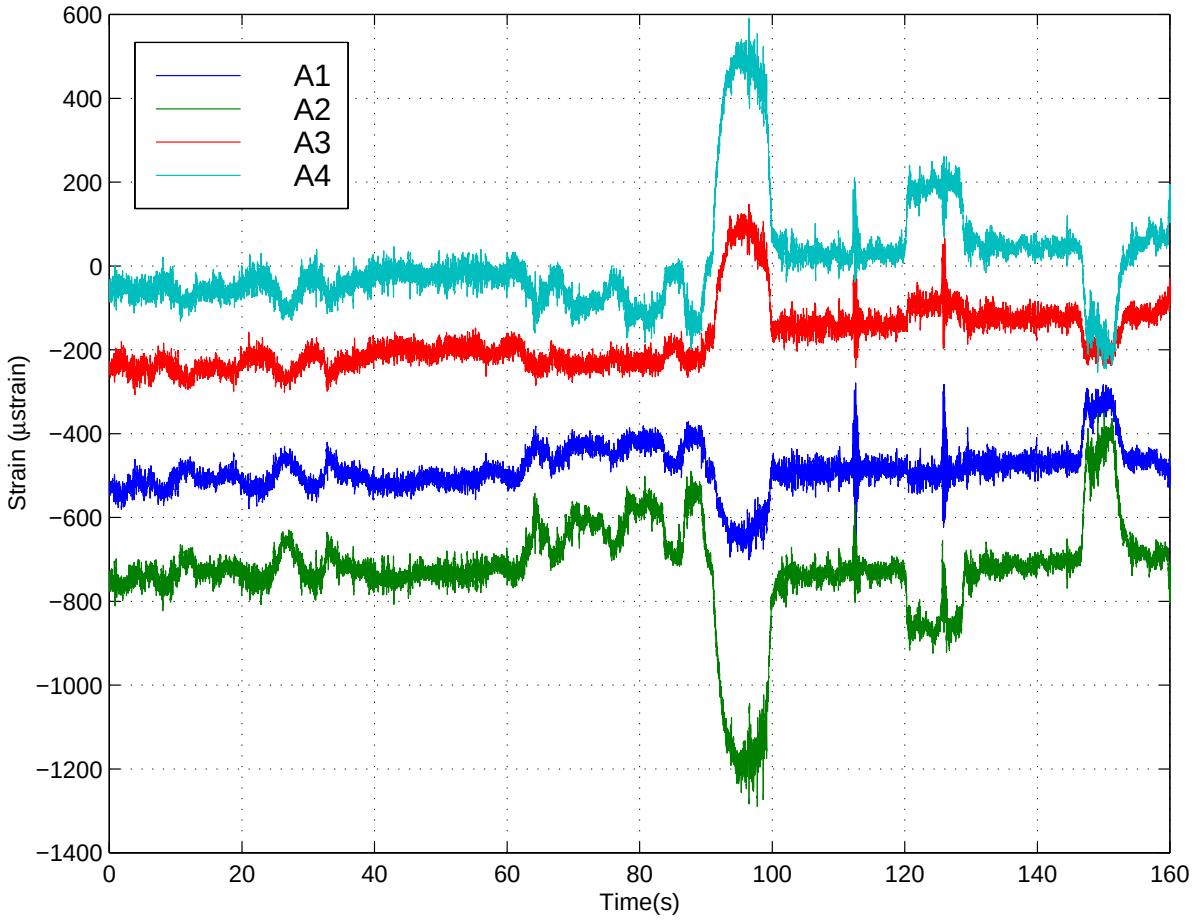

Figure 5.15 Data from the sensors mounted on the water jet tube; DC strain offsets have been added for greater clarity and do not represent real strain levels

The power spectra are dominated by the fundamental and higher harmonics of the waterjet, as we clearly see in Figure 5.16. In addition we find components at 2.4 and 3.5 Hz in the spectra of A1 and A3, while A2 and A4 have components at 6.4 and 7.2Hz.

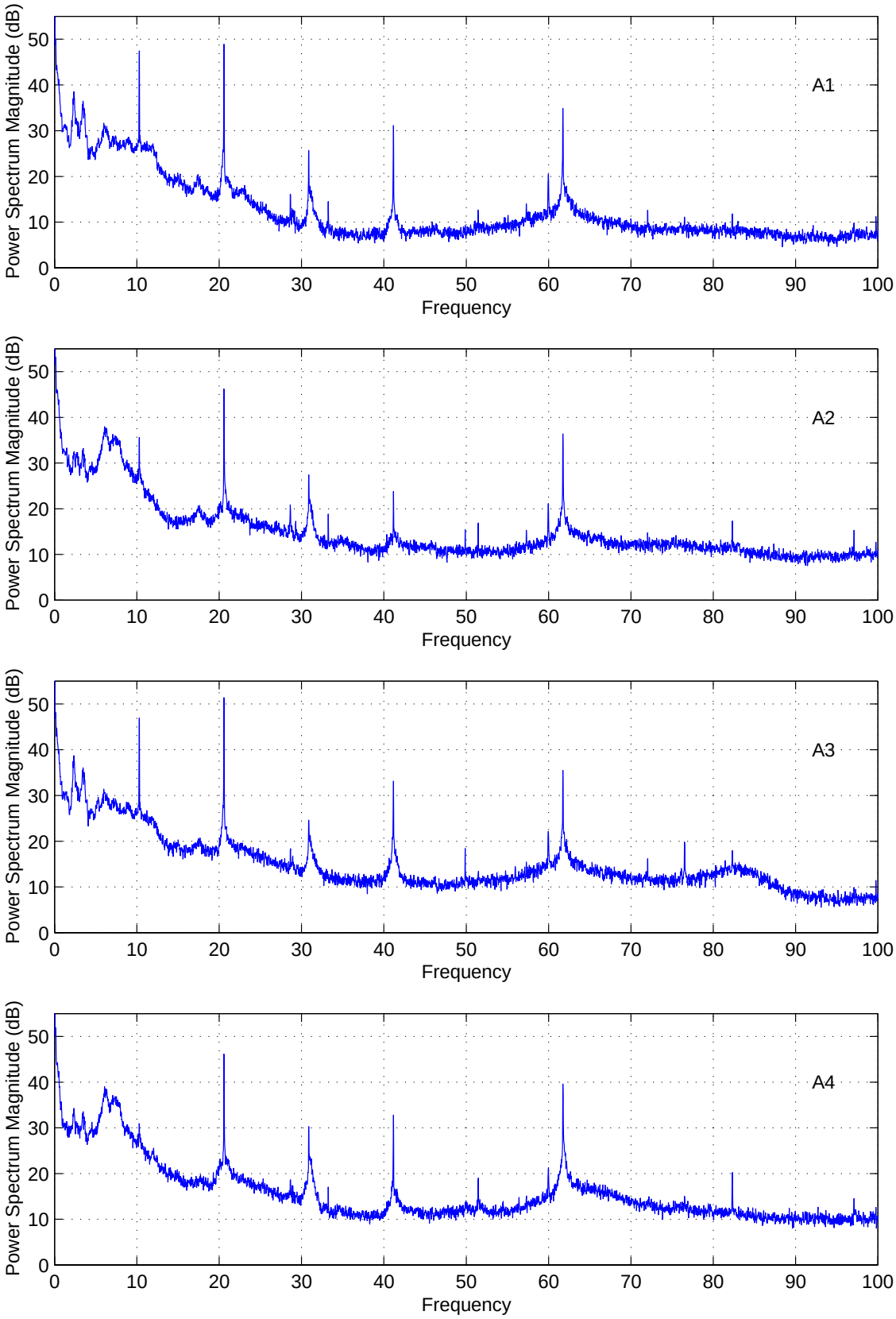

Figure 5.16 Power density spectra for the four sensors in array A on the waterjet

Array B on the wet deck mainly monitors for wet deck slamming, but the sea states were too low for any slamming to occur on this trip. However, we occasionally see significant strain transferred to the wet deck panel via a nearby bulkhead. An example is shown in Figure 5.17.

The transverse sensor placed closest to the bulkhead, B3, here sees a 2.4Hz transient with amplitude exceeding 100μstrain. This is not a mode of the wet deck panel, as we see from the fact that B3 and B2, which are placed perpendicularly, are not exactly 180° out of phase. We also notice that little of the 2.4Hz longitudinal bending mode is transferred to B2, which is mounted in the alongships direction. This leads us to believe that the wet deck is very close to the neutral axis for longitudinal bending.

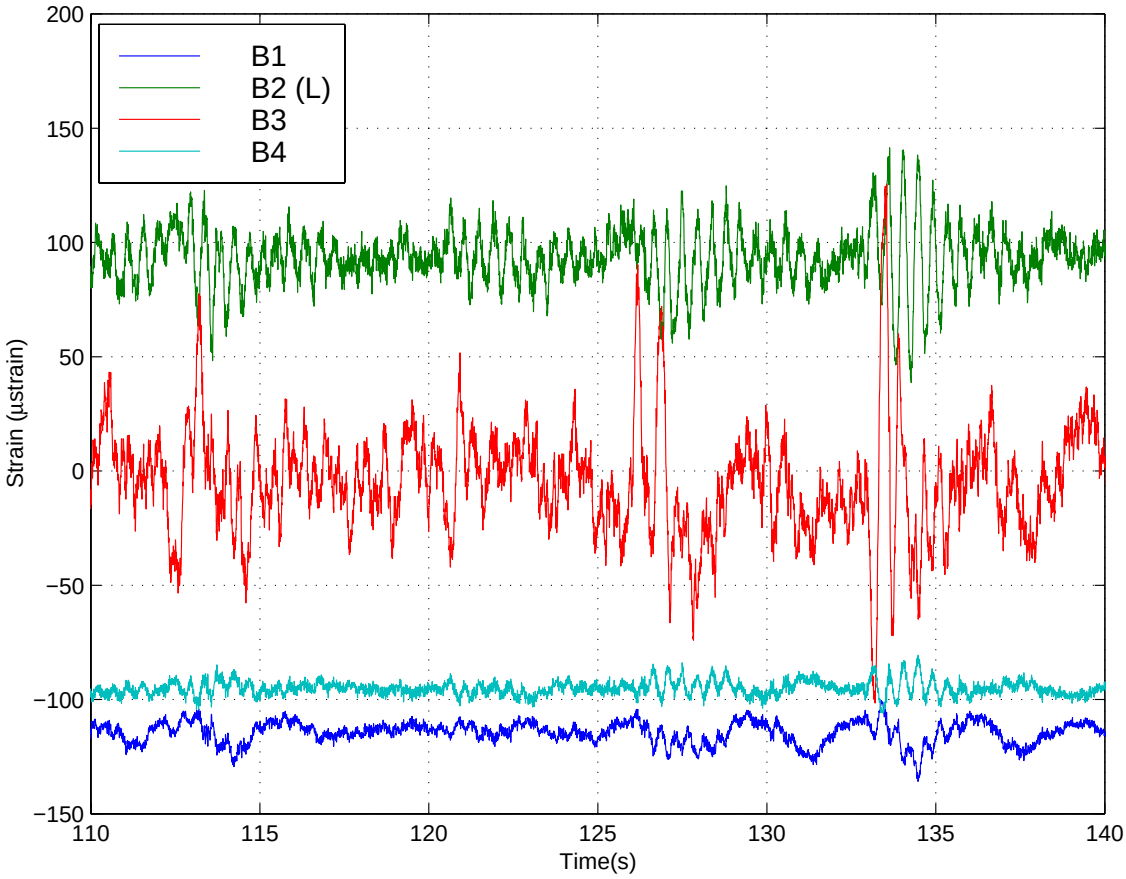

Figure 5.17 Data from array B on the wet deck; DC strain offsets have been added for greater clarity and do not represent real strain levels

Examples of data from the accelerometers are shown in Figure 5.18. The signal is completely dominated by the resonances of the accelerometers, and will have to be processed before we can extract any information. The domination of the resonances can also be seen from the power spectra in Figure 5.19.

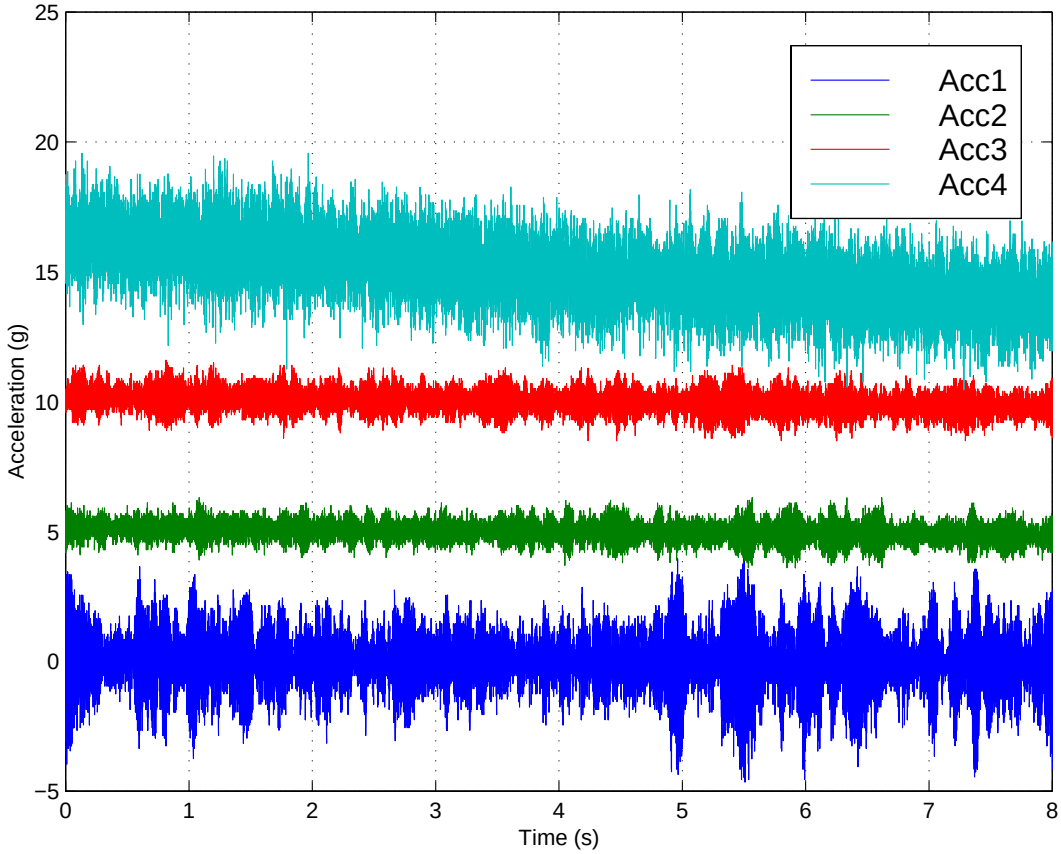

Figure 5.18 Accelerometer data

5.4 Maximum and minimum strain levels

To get an impression of the extreme amplitudes that can occur, we found the maximum and minimum strain value for each sensor in the data recorded on the trip from Kiel to Mandal. As mentioned above, the crew estimated the sea-state to be around 2. Table 5.1 shows the maximum and minimum strain level recorded, as well as the difference between the two. The difference represents an upper bound for the peak-to-peak amplitude.

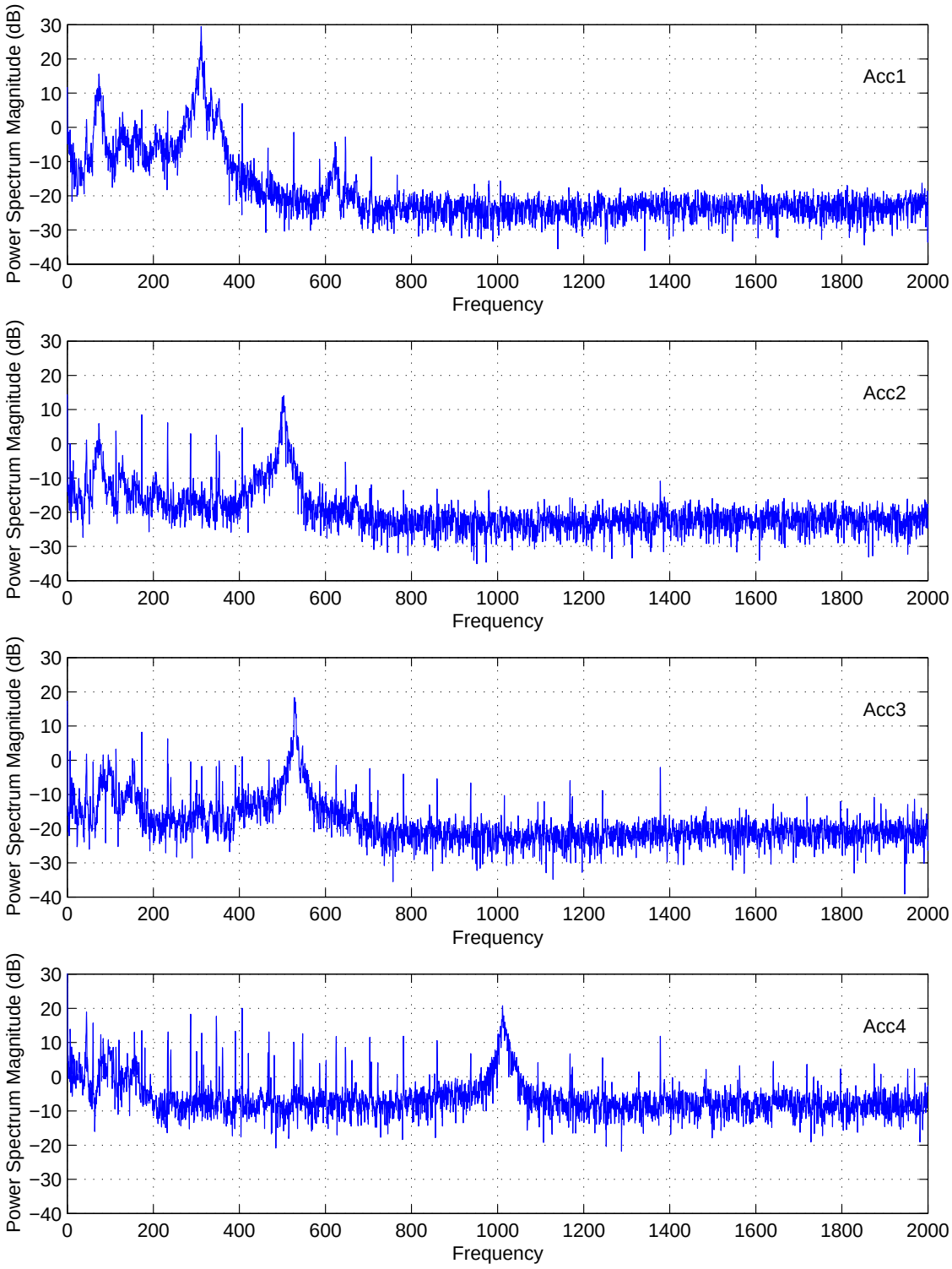

Figure 5.19 Accelerometer spectra showing the dominating natural frequencies of each sensor

Channel	Sensor	Max strain	Min strain	Peak-to-peak
2	**F2**	24.1	-37.0	61.1
3	**F3**	85.5	-74.1	159.6
4	**F4**	67.9	-64.3	132.2
5	**F5**	103.9	-114.8	218.7
6	**F6**	34.7	-58.7	93.4
7	**F7**	178.6	-164.1	342.7
8	**D1**	462.3	-303.4	765.7
9	**D2**	64.5	-53.3	117.8
10	**D3**	112.0	-224.9	336.9
11	**D4**	445.3	-231.9	677.2
12	**C1**	241.0	-437.9	678.9
13	**C2**	245.8	-404.9	650.7
14	**C3**	115.9	-66.9	182.8
15	**C4**	242.3	-66.1	308.4
16	**C5**	128.2	-73.2	201.4
17	**C6**	268.1	-420.6	688.7
18	**B4**	22.5	-21.0	43.5
19	**B3**	77.1	-51.4	128.5
20	**B2**	38.0	-51.6	89.6
21	**B1**	20.6	-18.0	38.6

Table 5.1 Maximum and minimum strain levels between Kiel and Mandal

6 MODE IDENTIFICATION

An initial effort has been made in order to identify the modes corresponding to the different frequency components in the data set. As an aid in this effort we have made a signal model that assumes that the signal from a given pair of sensors may be represented by an even (in-phase) and an odd (anti-phase) signal:

$$f_1(t) = f_e(t) + f_o(t)$$
$$f_2(t) = \mu(f_e(t) - f_o(t)) \qquad (6.1)$$

Here, $\mu = b/a$ represents the ratio of the two sensors' distance from the neutral axis for the bending modes and thus accounts for the difference in strain levels, see Figure 6.1. If we know the position of the neutral axis, or can find an estimate for μ, it is possible to estimate f_e and f_o. We propose to utilise the wavelet transform to do this.

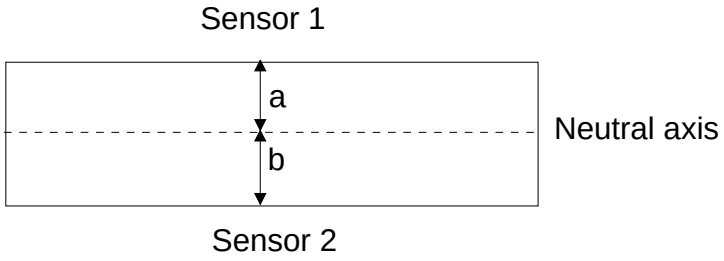

Figure 6.1 Simple model for bending measurements

Let *W* be the operator for the wavelet transform, and let *Wf* be the wavelet transform of the signal *f*. The wavelet transform can be visualised by a bank of bandpass filters, dividing the original signal into dyadic bands as illustrated in Figure 6.2. For more information about the wavelet transform see e g the reports by Urnes (5) or Bremer (6), or the book by Burrus (7).

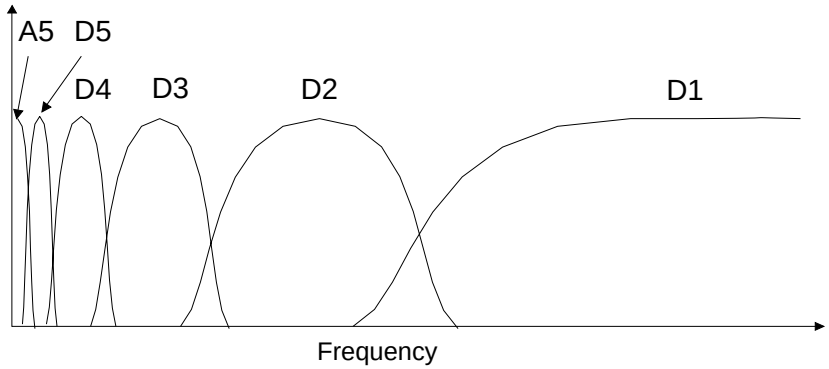

Figure 6.2 The wavelet transform resembles a bank of QMF filters that divide the frequency domain in dyadic bands named "D" for detail and a low frequency remainder named "A" for approximation

By taking a discrete wavelet transform we can separate the signal in different frequency bands, and then we can perhaps assume that in each band there is only one mode. One estimate for μ in the *i'*th band is then the ratio of the norm of the two signal sequences we are analysing:

$$ {}^{i}\mu = \frac{\left\| {}^{i}Wf_2 \right\|}{\left\| {}^{i}Wf_1 \right\|} = \frac{\left\| {}^{i}f_2 \right\|}{\left\| {}^{i}f_1 \right\|} \qquad (6.2) $$

The energy is conserved in the wavelet transform (there exists a Parseval's theorem for the transform), and this means that the ratio of the transform bands corresponds to the ratio of the signal energies at those frequencies, ie the signal amplitudes. The above expression automatically yields 1 if used on bands with even (compressive) modes, and the model is therefore valid even if μ is a meaningful concept in connection with bending modes only.

The single-band estimates for f_e and f_o are then

$$
\begin{aligned}
{}^{i}f_e(t) &= \frac{\mu_i\,{}^{i}f_1(t) + {}^{i}f_2(t)}{2\mu_i} \\
{}^{i}f_o(t) &= \frac{\mu_i\,{}^{i}f_1(t) - {}^{i}f_2(t)}{2\mu_i}
\end{aligned}
\qquad (6.3)
$$

We have implemented this algorithm in Matlab, where we take the wavelet transform, estimate μ in each band and then find the projections of the odd and even sequences on the different bands. These projections are time-domain sequences.

As an example we have tested the algorithm on data from sensors F5 and F6, where the odd modes will correspond to transverse bending modes. Figure 6.3 shows the original wavelet decomposition of the two data sequences, while the projections for the odd and even modes are shown in Figures 6.4 and 6.5. In Figure 6.3 we have plotted the time series corresponding to the energy in each wavelet band, and with the two signals shown in the topmost graph. From this figure we see that in the band labelled D4, which mainly contains energy in the frequency band 2.8-5.6Hz, the amplitude for F5 is much higher than that for F6. The same is true for band D5 covering frequencies in the range 1.4-2.8Hz.

Turning to the decomposition in an even and an odd mode, we show in the topmost graph in Figure 6.4 a best approximation to the anti-phase, or odd, components in the combined signals from F5 and F6. The other graphs show the projections of the individual bands on the time domain. The μ factor for each band is shown in the individual graphs, and we notice that the μs for the bands D4 and D5 that we remarked upon above, are very small compared to the others. This is an indication that the energy levels in the two channels at these frequencies are very different. Comparing the odd mode to the even mode shown in Figure6.5, we see that the in-phase strain level is significantly lower, and mainly concentrated at the lowest frequency.

We have found the power spectral density for the approximations to an odd and even mode, respectively. The spectra are shown in the lower half of Figure 6.6. By comparing them we may be able to identify the modal frequencies of the structural modes that were excited at the time. We notice that both spectra have a significant sub-Hz component that is likely to be the hull-wave interaction. The odd spectrum shows components at 3.5Hz and 6.5Hz that are not present to a significant degree in the even spectrum. Besides these frequencies we see only small features in the two spectra.

The presence of odd frequency components indicates a transverse bending mode in this case, but can we be certain that both the 3.5Hz and the 6.5Hz components correspond to such a mode? On reflection we realise that any frequency component that is present in only one of the channels will appear as an odd mode in the decomposition. To investigate this we have found the power spectral density for the two channels, as shown in the upper half of Figure 6.6. Comparing these two spectra we notice that at 6.5Hz the power level in the two channels are almost identical, while the 3.5Hz component is very different in the two. This suggests that we have a transverse bending mode at 6.5Hz, while the 3.5Hz component has a different origin.

The absence of any even components corresponding to compression modes is perhaps not surprising. The highly asymmetric nature of the exciting forces (from the sea) will favour the bending modes.

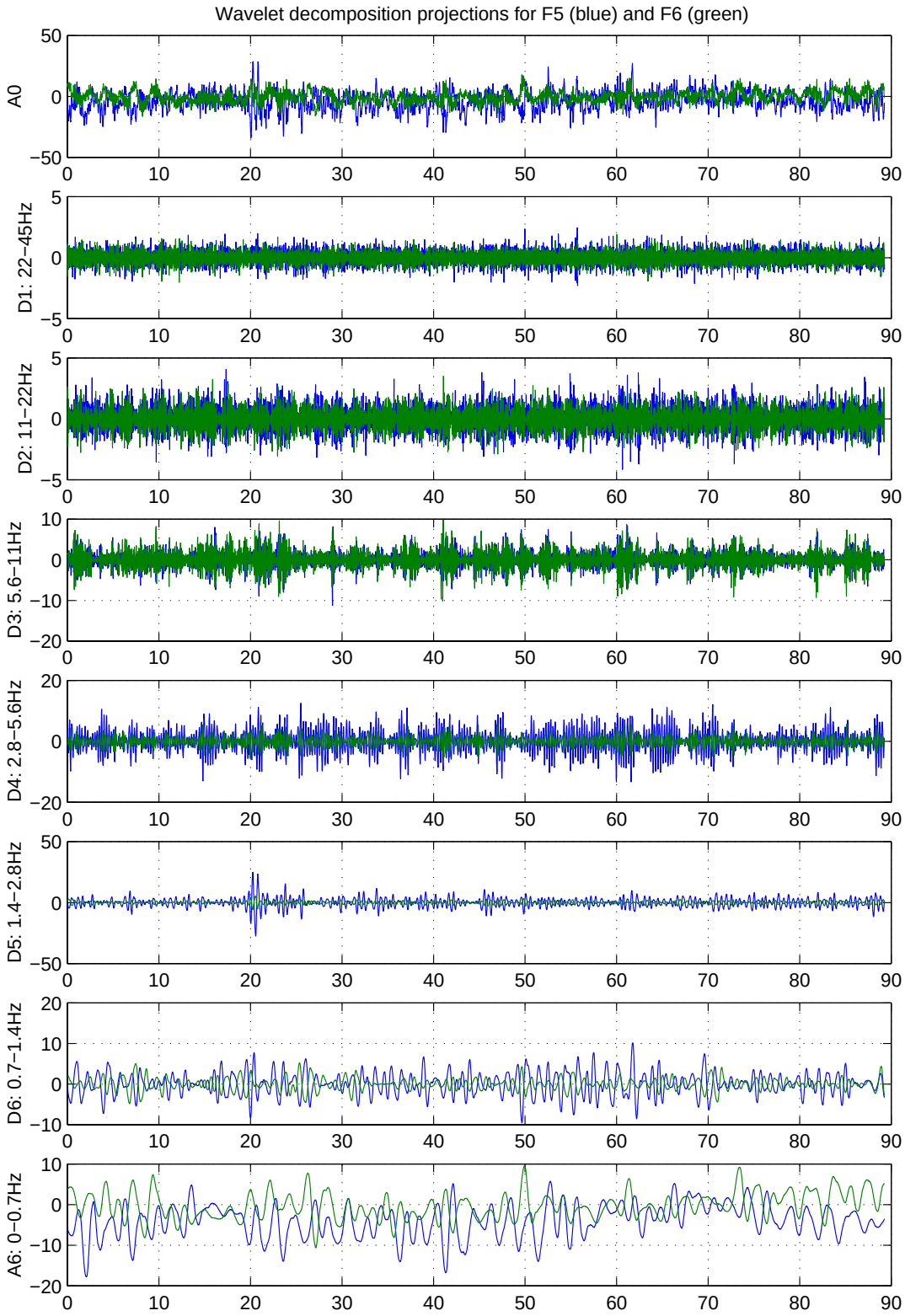

Figure 6.3 Wavelet decomposition for sensors F5 and F6

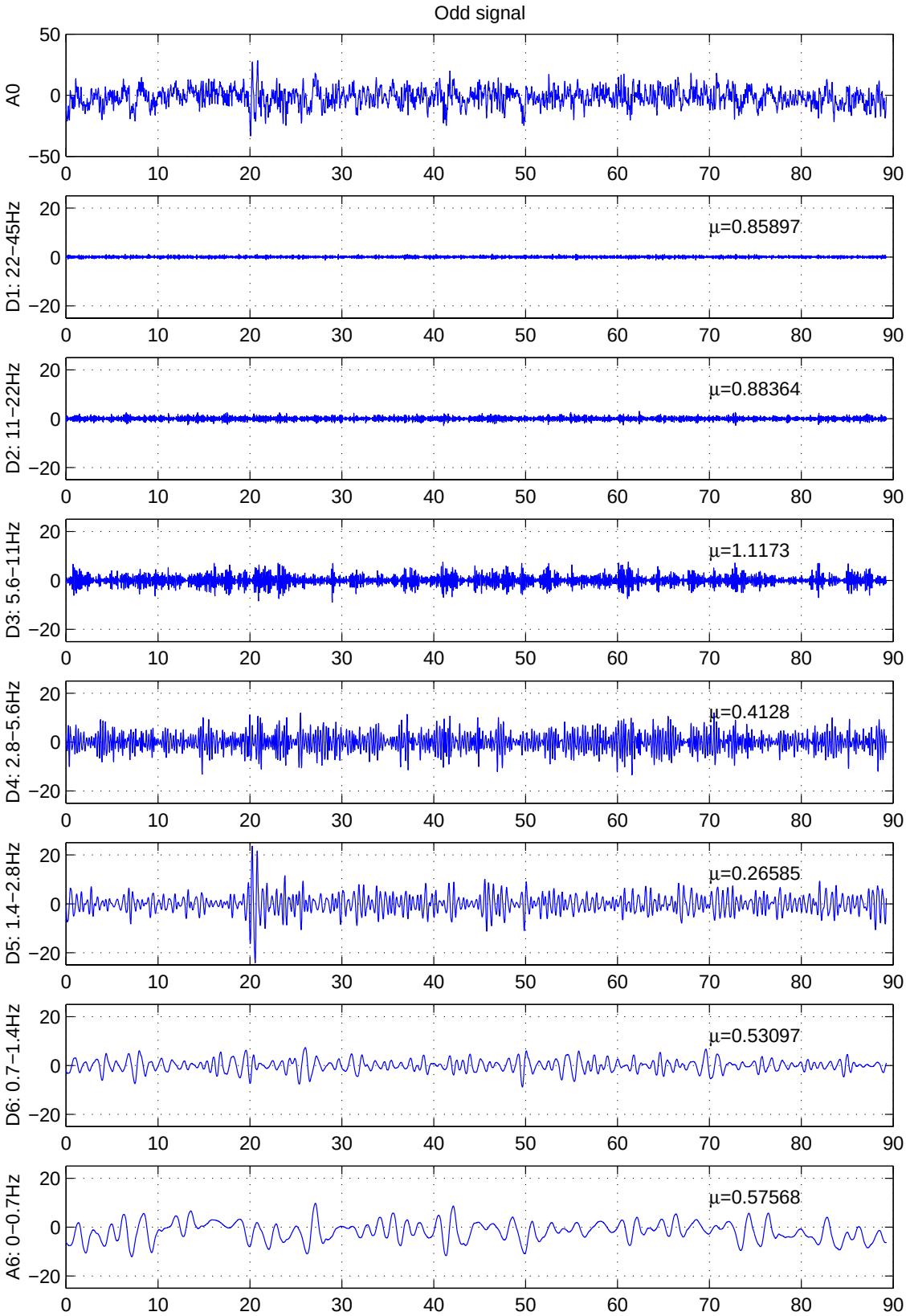

Figure 6.4 Odd components in signals from F5 and F6 indicating transverse bending

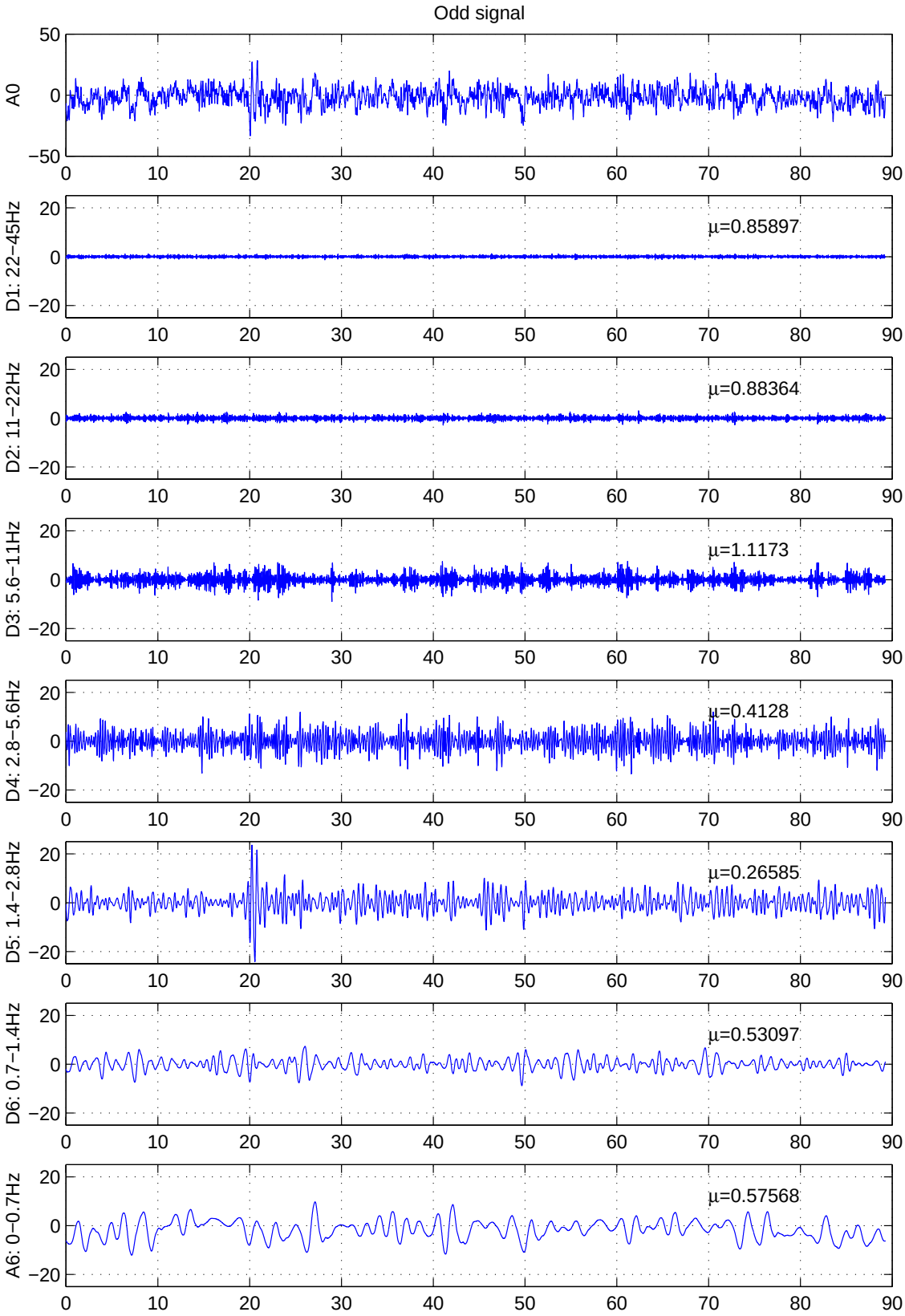

Figure 6.5 Even components in signals from F5 and F6 indicating transverse compression

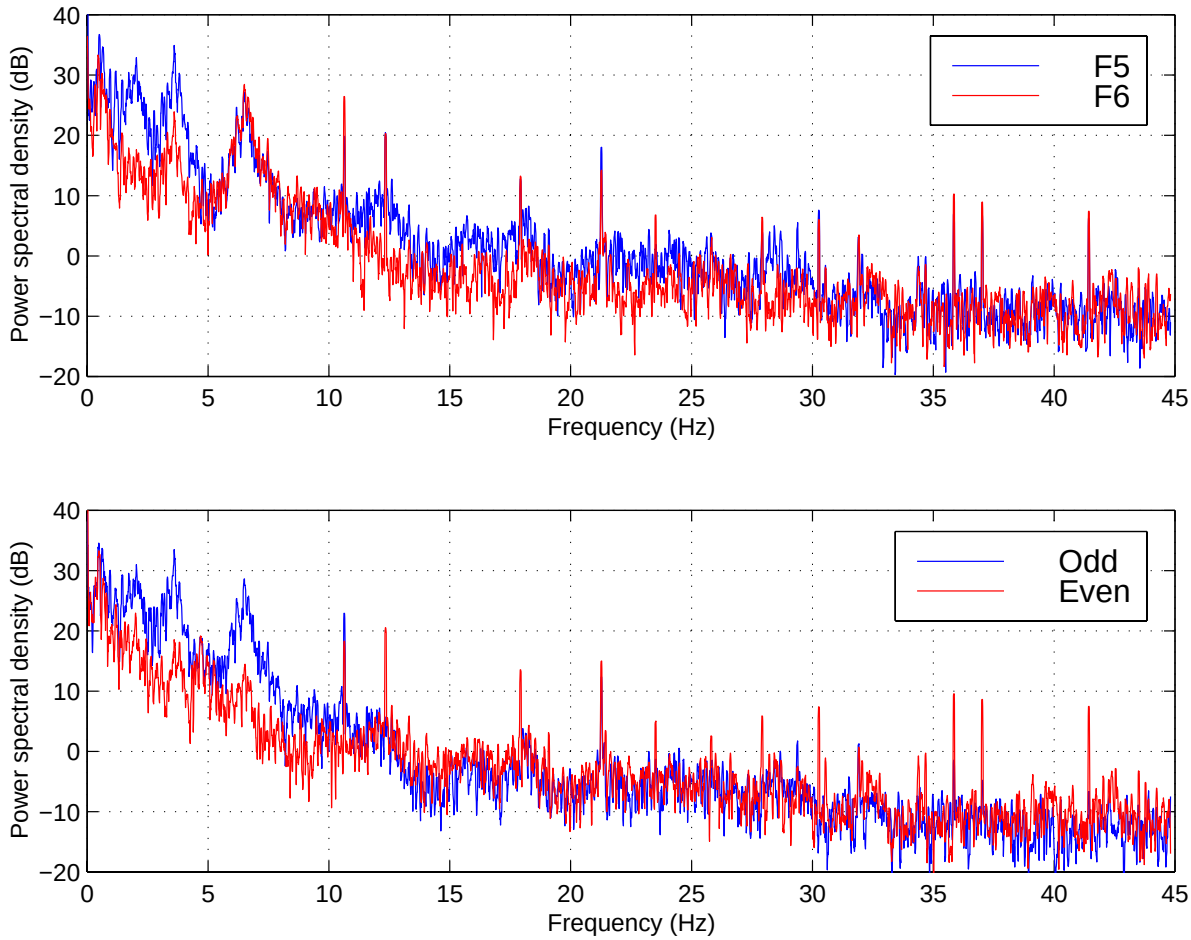

Figure 6.6 *Power density spectrum for the strain signal from F5 and F6 (top); power density spectrum for the odd and even parts of the signals from F5 and F6 (bottom)*

The longitudinal modes can be found from sensors D4 and C1, and Figures 6.8-6.11 illustrate the decomposition of these signals in even and odd modes.

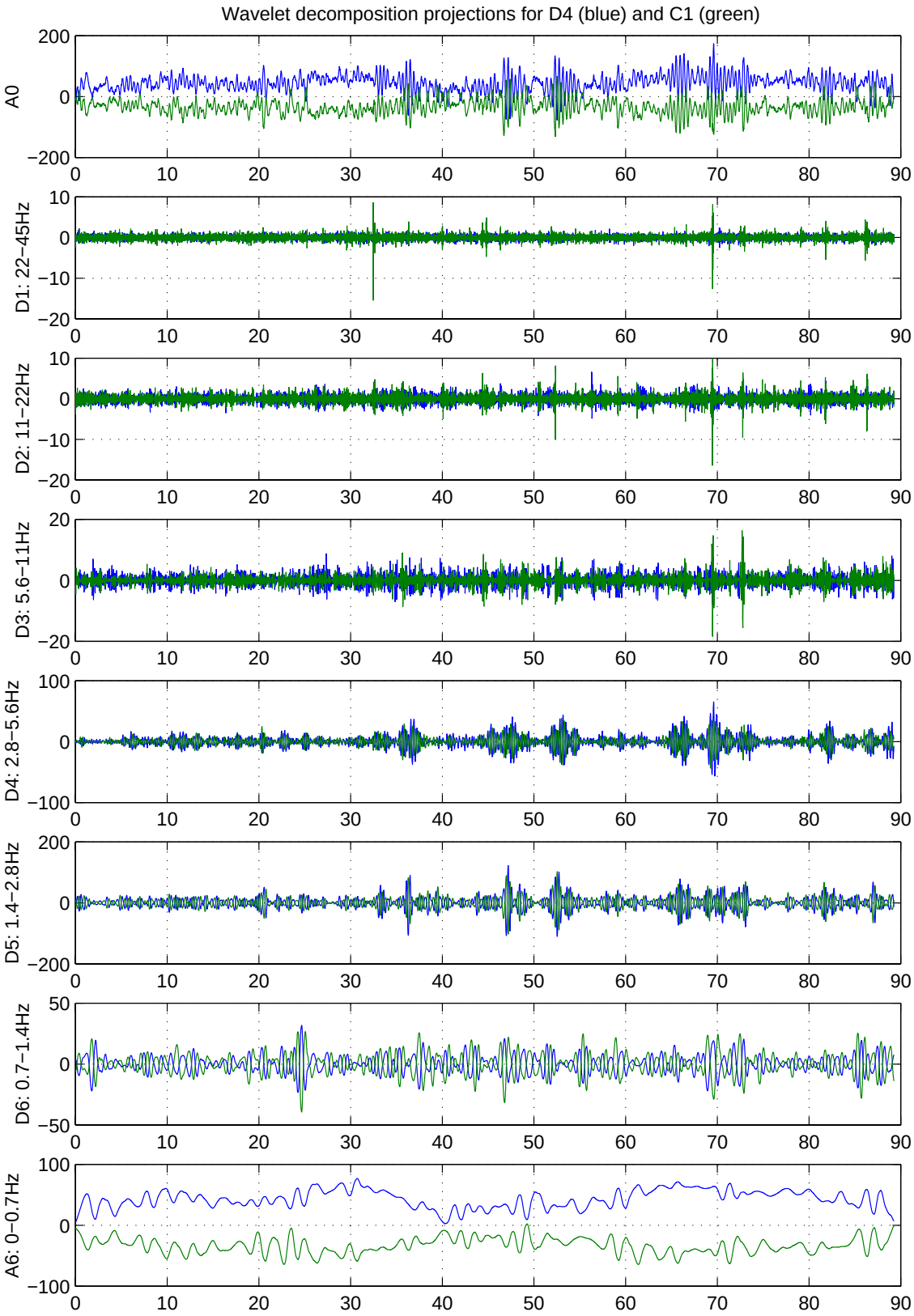

Figure 6.7 The signals from D4 and C1 projected onto wavelet bands

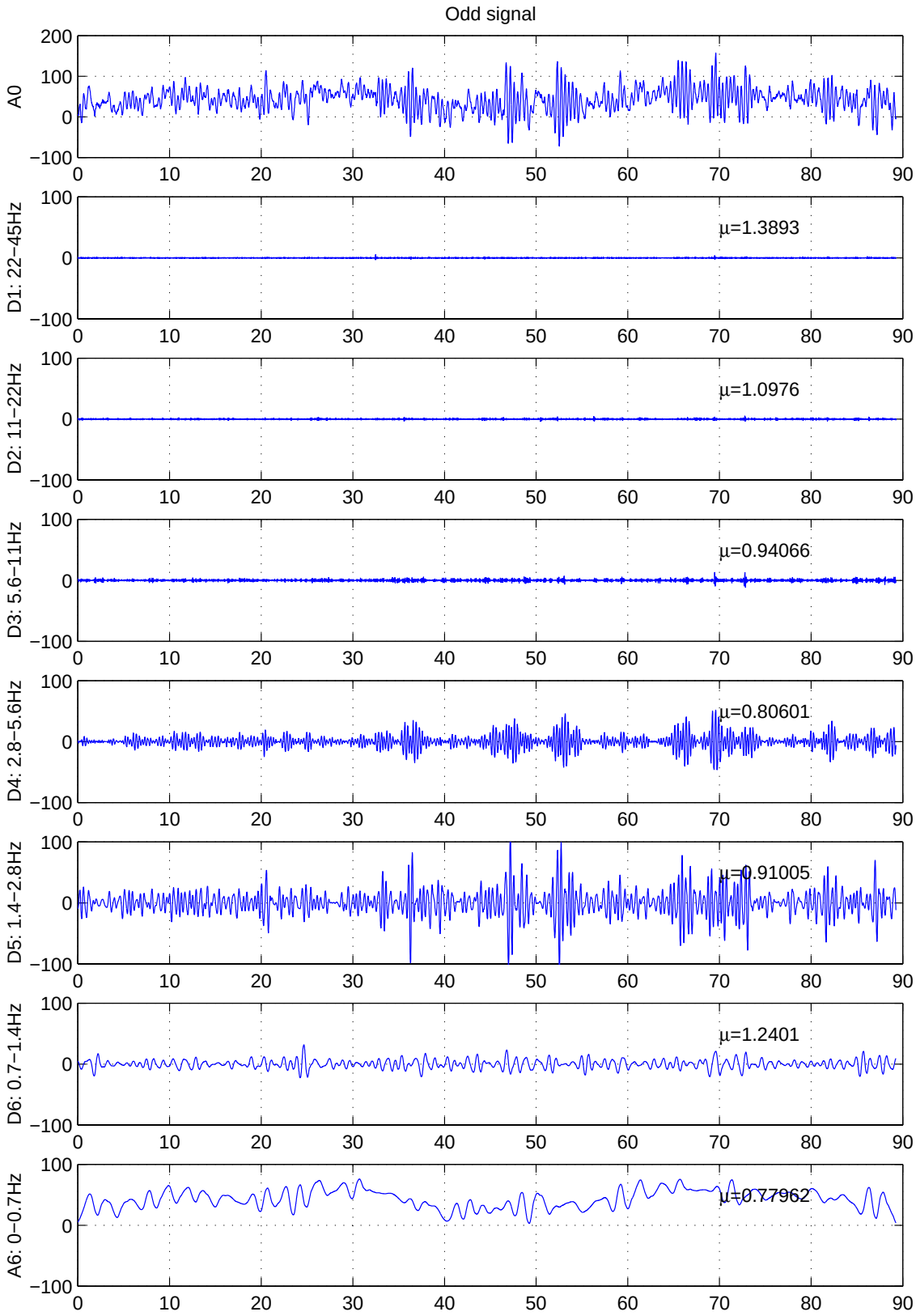

Figure 6.8 Odd components in signals from D4 and C1 indicating longitudinal bending

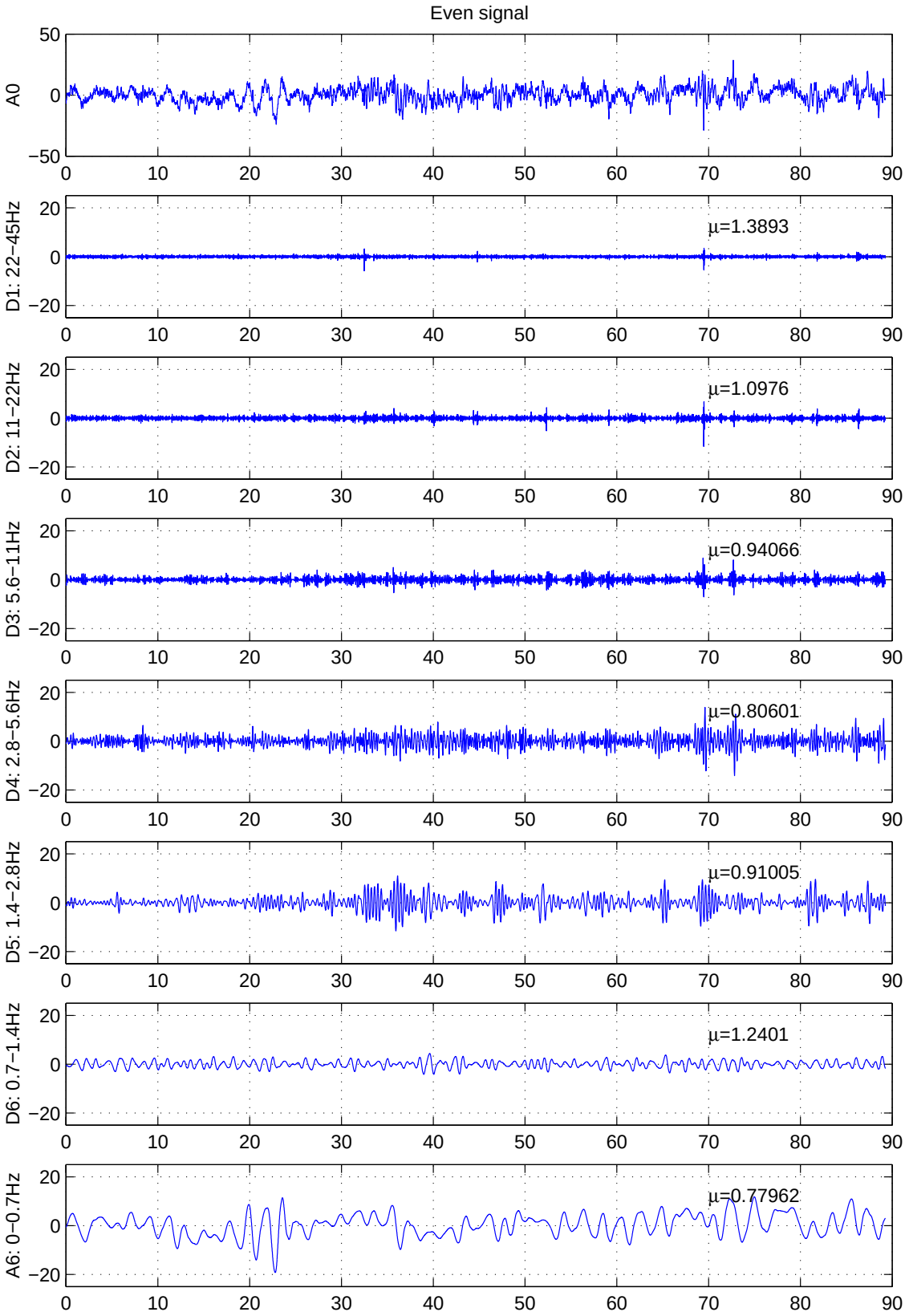

Figure 6.9 Even components in signals from D4 and C1 indicating longitudinal compression

We notice from the two spectra in Figure 6.10 that most of the energy is in the 2.4Hz longitudinal bending mode, while there is some energy in even modes at 2.9Hz and 4.8Hz.

The μ factors for the different bands are fairly close to 1, indicating that the two sensors are at a similar distance from the neutral axis.

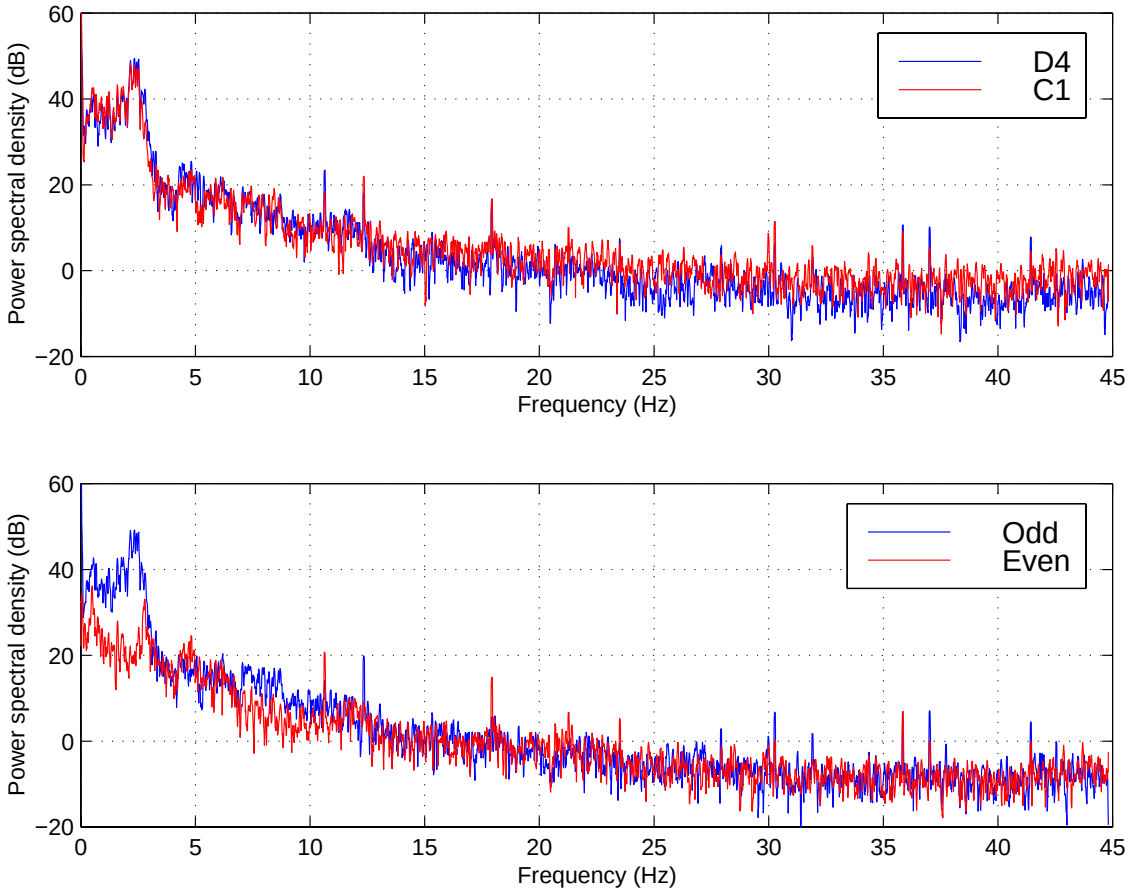

Figure 6.10 Power density spectra for the odd and even components in D4 and C1

A similar analysis of sensors D1 and E3 mounted on opposite sides of the deck in the alongships directions shows that these two sensors have odd modes at approximately 2.9Hz and 4.8Hz. This indicates that the even components in D4/C1 at 2.9Hz and 4.8Hz are due to a sideways bending of the hull that we have called wagging.

We have, finally, estimated μ in a sequence of data sets in order to evaluate the stability of the estimates. We cannot rule out that the position of the physical neutral axis will vary with the type of load, but if the estimate for μ shows a limited variation we can implement a simpler algorithm for the estimation of modal amplitudes. Figure 6.11 shows the estimate for μ in data sets from sensors F5 and F6 in the three lower frequency detail bands. The upper frequency bands contain mostly noise while the low frequency remainder is dominated by motions of the boat in waves, and therefore the estimates for μ are meaningless since this parameter is closely related to modes.

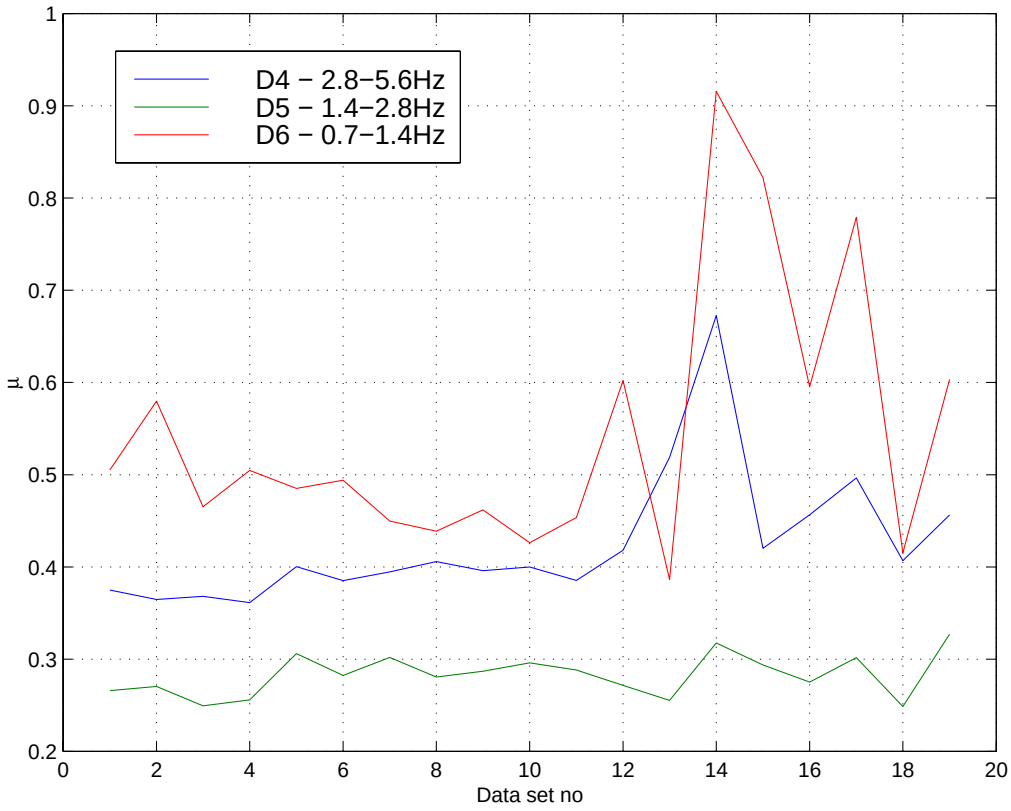

Figure 6.11 Estimates of μ for transverse bending obtained from a series of data sets for sensors F5 and F6

The estimated values for μ for sensors D4 and C1 are plotted in Figure 6.12, and again we only show the lower frequency detail bands. We see that for both F5/F6 and D4/C1 there are variations in the values for μ. The source of these variations is the different local strains measured by the two sensors. We have previously pointed out the problem of signals present in only one channel appearing as odd modes. These same single channel signals will systematically increase or decrease μ from its true value.

If this technique is to be used for repeated analyses, we recommend obtaining the real position of the neutral axis, or to find the upper or lower bounding value for μ. There is still the problem of single channel signals to deal with before the analysis is completely automated. However, the method has already aided us in the initial data analysis.

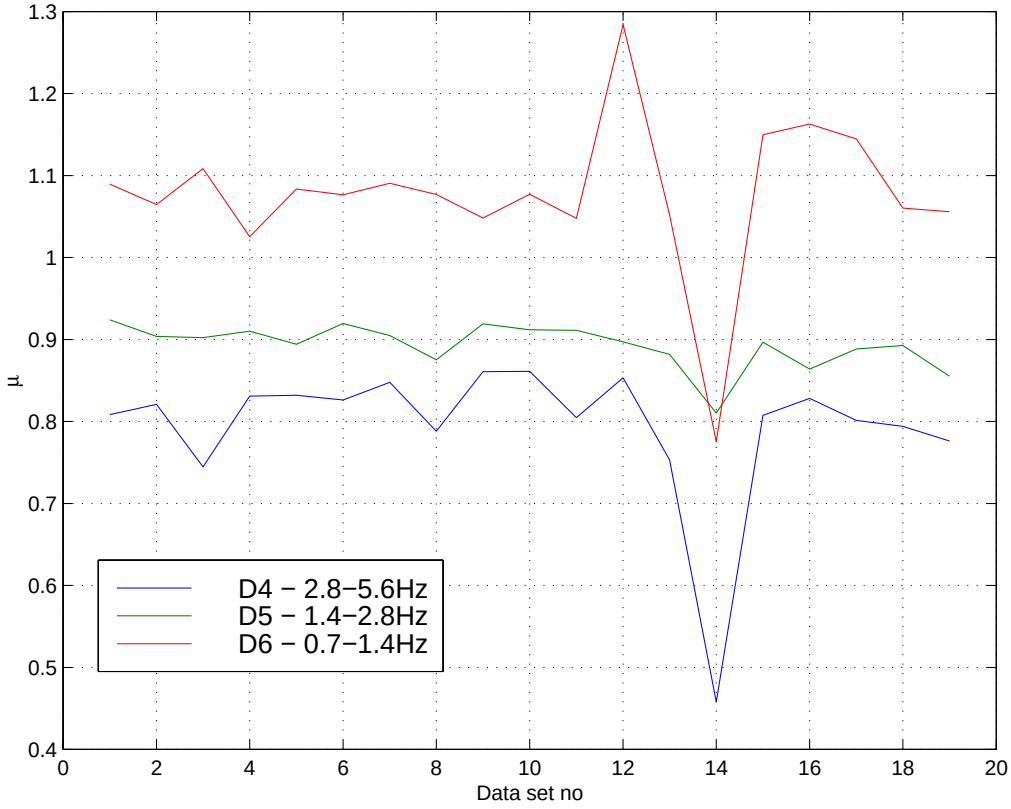

Figure 6.12 Estimates of μ for longitudinal bending obtained from a series of data sets for sensors D4 and C1

7 DISCUSSION

The results found with the Fabry-Perot system show that there are slowly varying strains that can have large amplitudes. On the other hand, we have so far not seen any indication that the higher bandwidth of the interferometric interrogation system is necessary. More detailed analyses of the high frequency signals should be carried out to ascertain this, so that a decision can be made on whether or not the interferometric interrogation adds value to the sensor system.

The data from the Fabry-Perot often contains spikes caused by a readout error in the scanning filter. We attribute this to poor splices between the photosensitive fibre with the gratings and the standard fibre used for the cabling. The poor quality of the splices is due to differences in numerical aperture, and leads to low power levels for some gratings in arrays that have standard fibre spliced into them. This in turn makes it difficult to set a threshold level in the Fabry-Perot system, since noise in the detection of a high power reflection could be interpreted as a low power reflection. These errors affect only a single sample at a time, but often lead to incorrect maximum strain levels, and the possibility of erroneous, high levels of tensile or compressive strain will have to be accounted for in the signal processing algorithms.

7.1 On the modes

We have postulated six different types of global modes for the MCMV vessel: Longitudinal bending in two planes (hog/sag and wagging), longitudinal compression, transverse bending, transverse compression, and torsion. In the present report we have attempted to identify the modal frequencies associated with these modes by comparing the response of the different sensor elements. Our findings are summarised in Table 7.1.

Mode	Fundamental freq	Higher order
Longitudinal bending (sag/hog)	2.4 Hz	7.5-8.5 Hz
Longitudinal bending (wagging)	2.9 Hz	4.9 Hz
Longitudinal compression	-	-
Transverse bending	6.4 Hz	-
Transverse compression	-	-
Torsion	2.7 Hz	-

Table 7.1 Modal frequencies

The higher order sag/hog mode observed is much smaller than the fundamental component, and only appears when the strain levels are fairly high. This could be a third order mode that is difficult to excite. The sensors are placed in, or very near, the node for a second order longitudinal bending mode. The wagging modes are also small compared to the fundamental sag/hog, which is reasonable since the forces available to excite these modes are much smaller. We have not observed longitudinal compression.

We have observed a component at 3.5Hz that may be transverse bending, but power levels in the two channels are very different, whereas they are identical for the 6.4Hz mode. We have not seen any transversal compression modes.

Nothing conclusive can be said about the torsional mode. We have found a component at 2.7Hz that is consistent with a torsional mode, but it is weak and appears rather seldom in the data set. Sensor D2, which we would expect to measure torsion, shows significantly lower strain levels than the neighbouring sensors, and the power spectrum is slightly different. This could be due to problems with low temperature and the presence of water during mounting of the grating.

We have observed only a few instances of panel vibrations in the bottom panel. This is probably due to the low sea state. The waves simply did not impact the hull with enough force to properly excite the panel vibrations at 17-20Hz.

We are mostly able to find the waterjet frequency in all channels at all times. At this time no air cushion frequencies have been identified, although a fairly strong component at 60Hz in

the wet deck sensors is a candidate. This frequency cannot be monitored at sampling rates of 90Hz, and it is a question whether the FP sampling rate should be increased to it's maximum at 360Hz.

On the trip from Kiel to Mandal we see a new frequency component at 1.5-1.7Hz that sometimes dominates over the longitudinal bending at 2.4Hz. It is unclear whether this is due to slightly different sea conditions or whether the damage on the hull could have caused the appearance.

In addition to the energy in the different modes, high strain amplitudes are associated with sub-Hz components that are due to wave-hull interaction.

7.2 On sensor placement

D4 and C1 are well placed to pick up the fundamental longitudinal bending. The two sensors measure the maximum strain levels due to longitudinal bending, which is useful. It is unclear whether we have seen the second or third order longitudinal bending mode. Although C2 and C6 were placed some distance from C1 they were still fairly close to amidships. If we wish to measure all longitudinal modes reliably, we should probably place a set of sensors closer to the bow.

The wet deck sensors measure very low strain levels, suggesting to us that the wet deck is close to the neutral axis for longitudinal bending. B3 shows the higher strain levels, but we believe that it mainly measures strain transferred via a bulkhead. The previous drop test (4) indicated that maximum slamming values can be seen in the plate centre, but that the strains are representative in other parts of the plate as well. The present results indicate that positioning the sensor in the plate centre is indeed beneficial, since this reduces the likelihood that the measured strains are transferred via the bulkheads.

The positions of F5 and F6 seem to be well suited for measuring transversal bending. However, it may also be interesting to place a corresponding pair of sensors near the bow where the waves can more easily excite bending directly with a hit on the side hulls.

Our present experience tells us that the rosettes in arrays D and E were not optimally placed for the sensing of torsion. Their position right in front of the casing is in a location with local strain components, and this complicates the signal analysis. One possibility is to replace the rosettes on deck with one rosette placed as exactly amidships as possible for easier measurement of torsion, with one grating alongships and the other two at $\pm 45°$.

8 CONCLUSIONS

The present field test has been a realistic test of a structure monitoring system. We have used a number of sensors that is of the same order of magnitude as the final CHESS system and we

are getting a grasp of how the data can be analysed in order to monitor the global flexures of a ship hull.

There are improvements to be made in the positioning of sensor elements to facilitate analysis with respect to global flexures. Still we have been able to identify modal frequencies for a large part of the expected global hull modes. It must also be considered that the whole test was carried out under very low sea-states, and we may have been able to identify more modes and other local vibrations if we had data for high sea-states as well.

We have demonstrated that the Fabry-Perot system can be left on board with only a minimum of crew monitoring, and still provide interesting data sets. We have also verified that the sensor elements are able to survive long periods on board. The cabling that was carried out in connection with this test will make it possible to quickly perform new tests at a later date, either to verify the condition of the sensors and cabling or to obtain data in rougher seas.

References

(1) Pran K & al (1998): Results of an initial sea-test for the Composite Hull Embedded Sensor System (CHESS), FFI/RAPPORT-98/05213, Approved for public release. Distribution unlimited.

(2) Dandridge A, Tveten A B, Giallorenzi T G (1982): Homodyne demodulation scheme for fiber optic sensors using phase generated carrier, *J Quantum Electronics* **18**, 10, 1647-1652.

(3) Bush I J & al (1992): TDM interferometric demodulation technique with 5 million samples per second capability In: *SPIE vol 1797 Distributed and multiplexed fiber optic sensors II*, 242-248.

(4) Havsgård G B & al (1998): Drop test with sandwich plate, FFI/RAPPORT-98/02009, Approved for public release. Distribution unlimited.

(5) Urnes E (1997): Wavelets and their use in the detection and characterization of transient signals, FFI/RAPPORT-97/03066, Approved for public release. Distribution unlimited.

(6) Bremer A (1998): Health monitoring of ship hulls using wavelets, wavelet packets and system identification techniques, FFI/RAPPORT-98/02764. Approved for public release. Distribution unlimited.

(7) Burrus C S, Gopinath R A, Guo H (1998): Introduction to wavelets and wavelet transforms, Prentice Hall, Upper Saddle River, NJ.

(8) Todd M D, Johnson G A, Althouse B A, Vohra S T (1998): Flexural beam-based fiber Bragg grating accelerometer, *IEEE Photonics Tech Lett* **10**, 11, 1605-1607.

DISTRIBUTION LIST

FFIE **Dato:** 1 november 1999

RAPPORTTYPE (KRYSS AV)	RAPPORT NR.	REFERANSE	RAPPORTENS DATO
X RAPP ☐ NOTAT ☐ RR	99/05425	FFIE/711/116	1 november 1999
RAPPORTENS BESKYTTEISESGRAD		ANTAll EKS UTSTEDT	ANTALL SIDER
UNCLASSIFIED		50	55
RAPPORTENS TITTEL		FORFATTER(E)	
FIELD TEST WITH A FIBRE OPTIC SENSOR SYSTEM ON A MINE COUNTER-MEASURE VESSEL		PRAN Karianne, HAVSGÅRD Geir Bjarte, WANG Gunnar, JOHNSON Gregg, DANVER Bruce, VOHRA Sandeep	
FORDELING GODKJENT AV FORSKNINGSSJEF:		FORDELING GODKJENT AV AVDELINGSSJEF:	

EKSTERN FORDELING

ANTALL	EKS NR	TIL
1		Fiber Optic Smart Strctures Section
1		V/ Sandeep Vohra
1		V/ Gary Cogdell
1		V/ Gregg Johnson
		Code 5600
		Naval Research Laboratory
		Washington DC 20375
		USA
1		FiReCo as
1		V/ Jon Taby
1		V/ Alf Egil Jensen
		Mosseveien 39B
		1610 FREDRIKSTAD
1		MARINTEK
1		V/ Ole Hermundstad
		Postboks 4125 Valentinlyst
		7002 TRONDHEIM
1		SFK, Teknisk Avdeling
1		V/ Atle Sannes
		Postboks 3 Haakonsvern
		5086 BERGEN
1		Kværner Mandal AS
1		V/ Nere Skomedal
		Postboks 283
		4501 MANDAL

INTERN FORDELING

ANTALL	EKS NR	TIL
14		FFI-Bibl
1		Adm direktør/stabssjef
1		FFIE
1		FFISYS
1		FFIBM
1		Gunnar Wang, FFIE
1		Geir Bjarte Havsgård, FFIE
1		Karianne Pran, FFIE
1		Geir Sagvolden, FFIE
1		Øystein Farsund, FFIE
12		Arkiv FFIE

FFI-K1 Retningslinjer for fordeling og forsendelse er gitt i Oraklet, Bind I, Bestemmelser om publikasjoner for Forsvarets forskningsinstitutt, pkt 2 og 5. Benytt ny side om nødvendig.

EKSTERN FORDELING **INTERN FORDELING**

ANTALL	EKS NR	TIL	ANTALL	EKS NR	TIL
1		Det Norske Veritas			
1		V/ Kåre Lindemann			
		DNV VTP 270			
		Veritasveien 1			
		1322 HØVIK			